CaMKIIα Expression Defines Two Functionally Distinct Populations of Granule Cells Involved in Different Types of Odor Behavior

Sarah Malvaut, Simon Gribaudo, Delphine Hardy, Linda Suzanne David,
Laura Daroles, Simon Labrecque, Marie-Anne Lebel-Cormier, Zayna Chaker,
Daniel Coté, Paul de Koninck, et al.

CaMKIIα Expression Defines Two Functionally Distinct Populations of Granule Cells Involved in Different Types of Odor Behavior

Highlights

- CaMKIIα expression defines functionally distinct granule cells in the olfactory bulb

- CaMKIIα$^+$ granule cells receive weaker inhibitory inputs than CaMKIIα$^-$ cells

- CaMKIIα$^-$ granule cells are involved in perceptual learning

- CaMKIIα$^+$ cells are essential for spontaneous and go/no-go odor discrimination

Authors

Sarah Malvaut, Simona Gribaudo, Delphine Hardy, ..., Alain Trembleau, Isabelle Caille, Armen Saghatelyan

Correspondence

isabelle.caille@upmc.fr (I.C.),
armen.saghatelyan@fmed.ulaval.ca
(A.S.)

In Brief

Malvaut et al. show that CaMKIIα expression defines functionally distinct granule cell (GC) subtypes in the olfactory bulb. CaMKIIα$^+$ GCs receive weaker inhibitory inputs and are preferentially activated by sensory inputs. CaMKIIα$^+$ and CaMKIIα$^-$ GCs are differentially recruited and play distinct roles during different odor tasks.

CaMKIIα Expression Defines Two Functionally Distinct Populations of Granule Cells Involved in Different Types of Odor Behavior

Sarah Malvaut,[1] Simona Gribaudo,[2,7] Delphine Hardy,[1,7] Linda Suzanne David,[1] Laura Daroles,[2] Simon Labrecque,[1] Marie-Anne Lebel-Cormier,[1] Zayna Chaker,[4,8] Daniel Coté,[1,5] Paul De Koninck,[1,5] Martin Holzenberger,[4] Alain Trembleau,[2] Isabelle Caille,[2,3,*] and Armen Saghatelyan[1,6,9,*]

[1]CERVO Brain Research Center, Quebec City, QC G1J 2G3, Canada
[2]Sorbonne Universités, UPMC Université Paris 06, INSERM, CNRS, Institut de Biologie Paris Seine, Neuroscience Paris Seine, 75005 Paris, France
[3]Université Paris Diderot, Sorbonne Paris Cité, 75013 Paris, France
[4]INSERM and Sorbonne Universités, UPMC, Centre de Recherche Saint-Antoine, Paris, France
[5]Faculté des Sciences et de Génie, Université Laval, Quebec City, QC G1V 0A6, Canada
[6]Department of Psychiatry and Neuroscience, Université Laval, Quebec City, QC G1V 0A6, Canada
[7]These authors contributed equally
[8]Present address: ZC, Biozentrum, University of Basel, Basel 4056, Switzerland
[9]Lead Contact
*Correspondence: isabelle.caille@upmc.fr (I.C.), armen.saghatelyan@fmed.ulaval.ca (A.S.)

SUMMARY

Granule cells (GCs) in the olfactory bulb (OB) play an important role in odor information processing. Although they have been classified into various neurochemical subtypes, the functional roles of these subtypes remain unknown. We used in vivo two-photon Ca^{2+} imaging combined with cell-type-specific identification of GCs in the mouse OB to examine whether functionally distinct GC subtypes exist in the bulbar network. We showed that half of GCs express Ca^{2+}/calmodulin-dependent protein kinase IIα (CaMKIIα+) and that these neurons are preferentially activated by olfactory stimulation. The higher activity of CaMKIIα+ neurons is due to the weaker inhibitory input that they receive compared to their CaMKIIα-immunonegative (CaMKIIα−) counterparts. In line with these functional data, immunohistochemical analyses showed that 75%–90% of GCs expressing the immediate early gene *cFos* are CaMKIIα+ in naive animals and in mice that have been exposed to a novel odor and go/no-go operant conditioning, or that have been subjected to long-term associative memory and spontaneous habituation/dishabituation odor discrimination tasks. On the other hand, a perceptual learning task resulted in increased activation of CaMKIIα− cells. Pharmacogenetic inhibition of CaMKIIα+ GCs revealed that this subtype is involved in habituation/dishabituation and go/no-go odor discrimination, but not in perceptual learning. In contrast, pharmacogenetic inhibition of GCs in a subtype-independent manner affected perceptual learning. Our results indicate that functionally distinct populations of GCs exist in the OB and that they play distinct roles during different odor tasks.

INTRODUCTION

Granule cells (GCs) are the most abundant neuronal population in the olfactory bulb (OB) and largely outnumber bulbar principal neurons (mitral/tufted cells) [1]. They establish reciprocal dendro-dendritic synapses with the lateral dendrites of principal neurons and play a major role in odor information processing by synchronizing principal cell activity via lateral and recurrent inhibitions [2, 3]. The synchronization of principal neurons by GCs plays an important role in neuronal pattern separation by improving odor discrimination and disambiguating overlapping sensory maps evoked by similar odorants [4, 5]. In vivo two-photon Ca^{2+} imaging revealed, however, that odor responses by GCs are temporally and spatially heterogeneous [6]. The molecular and cellular mechanisms underlying such heterogeneous responses in GCs remain unclear.

Several GC subtypes have been identified based on immunohistochemical markers [7–11]. In addition, up to 15% of GCs are continuously renewed during adulthood [12–14], which adds another level of complexity. Adult-born neuronal precursors are derived from stem cells in the subventricular zone (SVZ) of the lateral ventricle. Following their migration along the rostral migratory stream (RMS) into the OB, approximately 95% differentiate into GCs [15–17]. Little is known about the neurochemical heterogeneity of adult-born GCs and, until now, studies aimed at understanding the roles of adult-born neurons in odor information processing have considered these cells as a homogeneous population [18–21]. However, it is conceivable that different subtypes of both early-born and adult-born GCs may be activated by distinct olfactory tasks and may play specific roles in different odor behaviors [22]. There is thus a need

to understand the exact contributions of specific GC subtypes to odor behavior.

In the present study, we used in vivo two-color, two-photon imaging to show that a higher proportion of CaMKIIα-immuno-positive (CaMKIIα⁺) GCs are spontaneously activated under baseline conditions and are more responsive to odor stimulation than CaMKIIα-immunonegative (CaMKIIα⁻) GCs. In line with our imaging data, our analysis of the expression of the immediate early gene *cFos* combined with an assessment of CaMKIIα immunolabeling revealed that 75%–90% of cFos-immunoreactive (cFos⁺) cells belong to the CaMKIIα⁺ GC subtype in naive mice as well as in mice that have been exposed to a novel odor stimulation, long-term associative odor memory, go/no-go operant conditioning, or spontaneous habituation/dishabituation odor discrimination tasks. This percentage decreased following an olfactory perceptual learning task, indicating that CaMKIIα⁻ GCs had been recruited. CaMKIIα⁺ GCs make up half of early-born and adult-born GCs and are morphologically indistinguishable from their CaMKIIα⁻ counterparts. In contrast, our electrophysiological recordings revealed that CaMKIIα⁺ GCs receive weaker inhibitory inputs, which may underlie their higher sensitivity to incoming sensory inputs. Pharmacogenetic inactivation of CaMKIIα⁺ GCs affected go/no-go and habituation/dishabituation odor discrimination, but not perceptual learning. On the other hand, subtype-independent pharmacogenetic inhibition of GCs impaired perceptual learning. Our results show that CaMKIIα⁺ GCs play an important role in processing odorant information in the basal state and during spontaneous and go/no-go odor discrimination, but not during perceptual learning, indicating that different subtypes of GCs make distinct functional contributions to specific odor behaviors.

RESULTS

Functionally Heterogeneous Populations of GCs in the Adult OB

To study the activity of GCs in vivo, we injected an AAV encoding the Ca²⁺ indicator GCaMP6s into the OB. Two to four weeks post-injection, we implanted a cranial window over the dorsal OB and investigated the Ca²⁺ responses of GCs in anesthetized mice under baseline conditions and following odor stimulation (Figures 1A and 1B). In line with and extending previous reports [6, 23], our in vivo Ca²⁺ imaging revealed the presence of functionally distinct subtypes of GCs based on their spontaneous activity. Slightly more than half of the GCs did not show any change in their fluorescence intensity during the 2-min acquisition period (30-Hz sampling rate; blue arrowhead in Figure 1C; top trace in Figure 1D). In contrast, 47.7% ± 2.9% of GCs displayed a clear spontaneous increase in fluorescence intensity (red arrowheads in Figure 1C; middle and bottom traces in Figure 1D; n = 608 cells from 8 animals; Figure 1E). To determine whether GC responses are modified by novel odor stimulations, we presented six structurally different odors that are known to activate the dorsal surface of the OB [6, 24, 25]. Odor stimulations resulted in an increase in Ca²⁺ levels in GCs (Figure 1F; Movie S1). In some GCs, the increase appeared during the 5-s odor presentation period (ON response), whereas in other GCs, Ca²⁺ levels increased after the end of the odor stimulation (OFF response; Figures 1F and 1G; Movie S1). The percentage of responsive cell-odor pairs for the ON and OFF responses were 40.6% ± 5.4% and 10.5% ± 1.7%, respectively (n = 1,937 cell-odor pairs from 6 mice; Figures 1H and 1I). The peak amplitude of responses (ΔF/F) was 50.2% ± 1.9%, and odor tuning (the number of odors eliciting responses from among the six odors tested) was 1.5 ± 0.09. These results suggest that functionally heterogeneous populations of GCs exist and that some are more prone to activation under both baseline conditions and following odor stimulation.

GCs Can Be Divided into Two Functionally Different Subtypes Based on the Expression of CaMKIIα

CaMKIIα plays a major role in different forms of synaptic plasticity and is highly expressed in the adult OB granule cell layer (GCL) [10, 11]. However, it is not known whether all GCs express CaMKIIα, including adult-born GCs, or whether there is a developmental shift in CaMKIIα expression during GC maturation. We thus quantified the percentage of CaMKIIα⁺ GCs by immunolabeling combined with either DAPI or neuronal marker (NeuN) staining and observed that 47.8% ± 1.4% of DAPI- and 50.8% ± 2.1% of NeuN-stained cells express CaMKIIα (Figures 2A–2C). To determine whether CaMKIIα is stably or transiently expressed in GCs, we analyzed CaMKIIα-tdTomato mice and found that the reporter is expressed by 66.5% ± 3.9% of the GC population (Figures 2B and 2C), irrespective of their location in the GCL (Figures 2D and 2E). In addition, 87.9% ± 2.6% of the tdTomato⁺ GCs were CaMKIIα⁺, indicating a stable expression of CaMKIIα. CaMKIIα was also expressed by nearly 50% of adult-born GCs labeled by the intraperitoneal injection of bromodeoxyuridine (BrdU), a DNA replication marker (Figures 2F and 2G). Because BrdU labels only a small cohort of adult-born neurons, we labeled larger populations of cells by injecting tamoxifen into adult NestinCreERT2::CC-GFP mice. Our results showed that 44.2% ± 3.0% of 4-week-old GFP⁺ adult-born neurons also express CaMKIIα (Figure 2G). These findings suggest that GCs can be divided into two equally represented CaMKIIα⁺ and CaMKIIα⁻ subtypes.

To determine whether these equally represented subtypes of GCs are functionally similar or not, we examined their activity using GCaMP6s and two-color, two-photon imaging. To discriminate the two populations, we co-injected GCaMP6s AAV under the ubiquitous CAG promoter with the CaMKIIα-Cre-mCherry and CAG-Flex-tdTomato AAV vectors. To determine the efficiency of viral infection, we quantified the percentage of red fluorescent protein (RFP) (mCherry or tdTomato)-expressing GCs that were CaMKIIα⁺. Our results revealed that 85.1% ± 0.8% of RFP-expressing (RFP⁺) GCs were CaMKIIα⁺ (n = 350 cells from 3 mice). Because our GCaMP6s vector was under the ubiquitous CAG promoter, we also observed that 48.5% ± 4.8% of GCaMP6s-infected cells were CaMKIIα⁺. Interestingly, our in vivo two-photon imaging data revealed functional differences between RFP⁺/GCaMP6s⁺ and RFP⁻/GCaMP6s⁺ GCs under baseline conditions. Whereas 59.6% ± 3.3% of RFP⁺/GCaMP6s⁺ GCs displayed a clear spontaneous increase in fluorescence intensity under baseline conditions, significantly fewer RFP⁻/GCaMP6s⁺ showed changes in the fluorescence intensity (44.3% ± 3.0%; n = 133 and n = 475 cells from 7 and 8 mice, respectively; p < 0.01; Figures 2H and 2I; Movie S2). Because RFP⁻/GCaMP6s⁺ cells were comprised of both CaMKIIα⁺ and
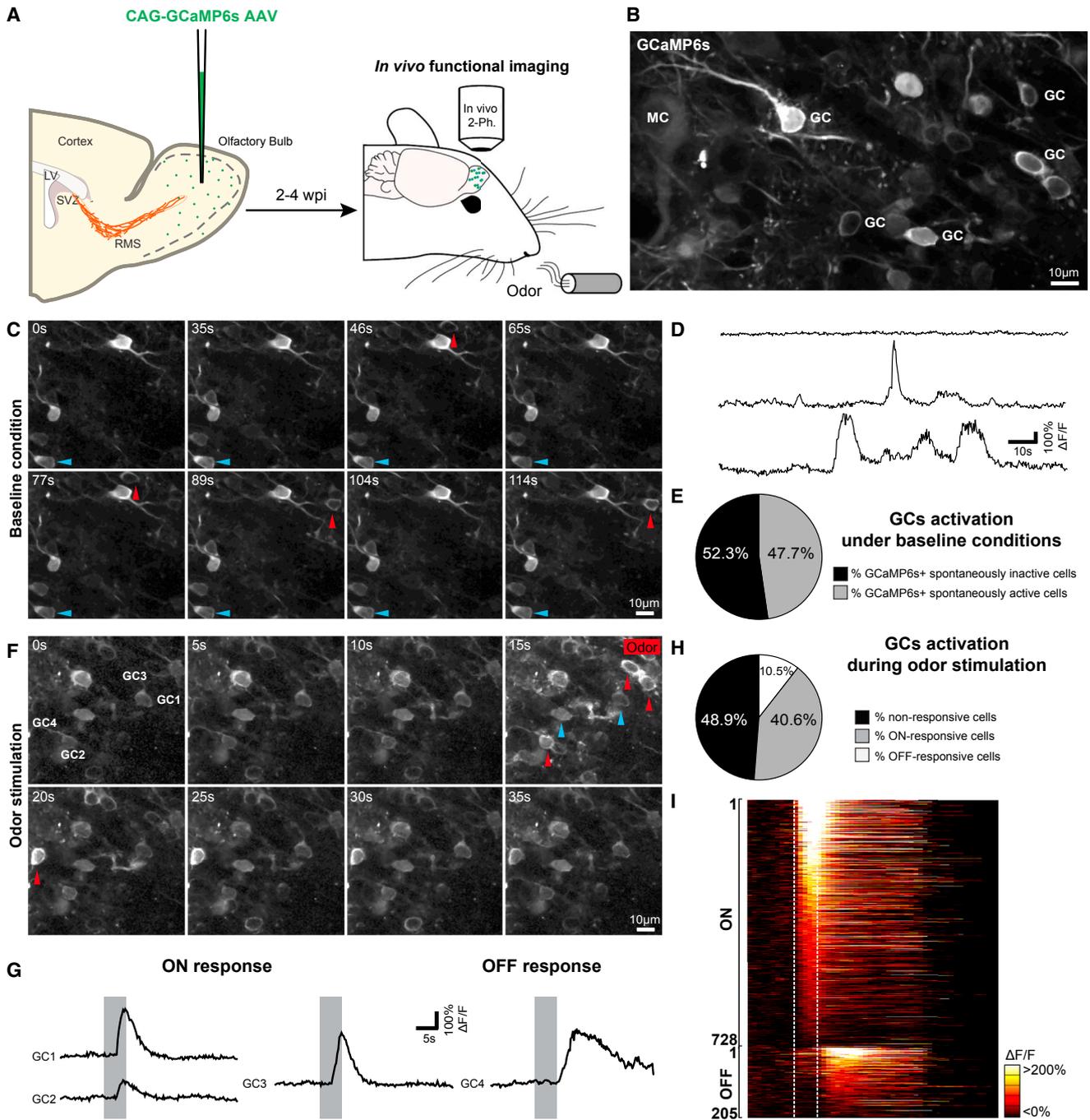
Figure 1. In Vivo Ca²⁺ Imaging of GC Activity under Baseline and Odor Stimulation Conditions

(A and B) Schematic representation (A) and representative two-photon image of in vivo Ca²⁺ imaging (B) 2–4 weeks after GCaMP6s-expressing AAV injection.

(C) Two-photon in vivo recordings of GC activity under baseline conditions. Red and blue arrowheads indicate cells with high and low baseline activity, respectively.

(D and E) Sample traces (D) and quantification (E) of cells recorded under baseline conditions.

(F) Representative images of in vivo Ca²⁺ imaging of GC activity during an odorant stimulation. The time is indicated in the upper left corner. The odor-application interval is indicated in the upper right corner. ON- or OFF-responsive GCs are indicated by red arrowheads, whereas non-responsive cells are indicated by blue arrowheads.

(G) Sample traces of ON- and OFF-responsive GCs. Odor application (5 s) is indicated by the gray box.

(H) GC activation following odor presentation, with the percentage of ON-, OFF-, and non-responsive cell odor pairs.

(I) Pseudo-colored heatmaps of ON- and OFF-responsive GCs are shown. Cell odor pairs are sorted according to the amplitude of their responses.
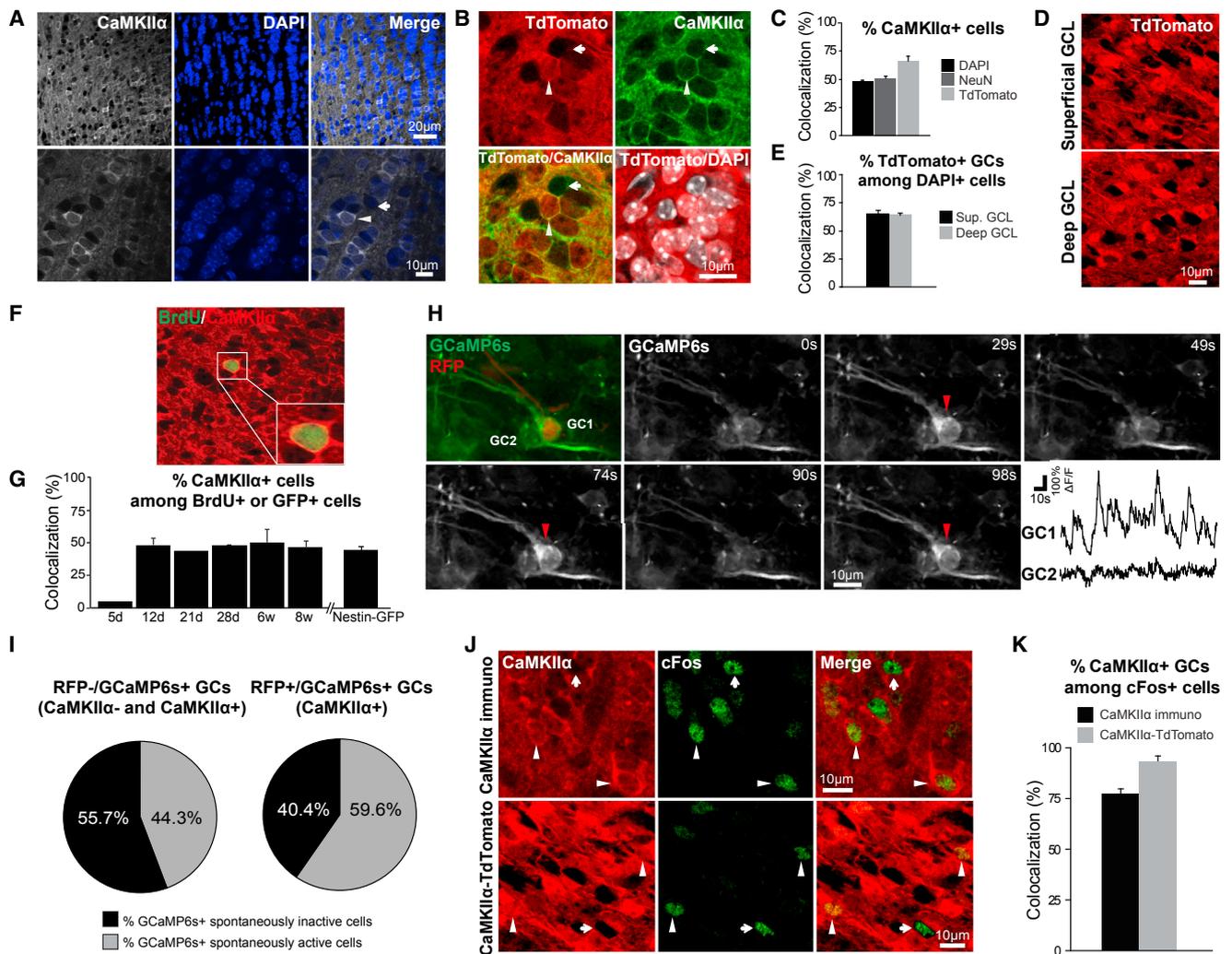
Figure 2. Expression of CaMKIIα in the Adult Olfactory Bulb

(A) Confocal images of CaMKIIα immunolabeling (white) and DAPI staining (blue) in the GCL. The bottom panel shows a higher magnification of the images in the upper panel. The arrow and arrowhead indicate CaMKIIα⁻ and CaMKIIα⁺ GCs, respectively.

(B) Confocal images of CaMKIIα-tdTomato-expressing cells (red), CaMKIIα immunolabeling (green), and DAPI staining (white) in the GCL. The arrow and arrowhead indicate CaMKIIα⁻ and CaMKIIα⁺ GCs, respectively.

(C) Quantification of the percentage of CaMKIIα⁺ GCs among DAPI⁺ (black) and NeuN⁺ (dark gray) cells in C57BL/6 mice and tdTomato⁺ GCs among DAPI⁺ (light gray) cells in CaMKIIα-tdTomato reporter mice.

(D and E) Confocal images (D) and quantification (E) of deep and superficial tdTomato⁺ GCs in CaMKIIα-tdTomato reporter mice.

(F) Confocal images of a 21-day-old BrdU⁺ GC (green) that also expresses CaMKIIα (red).

(G) Quantification of the percentages of adult-born CaMKIIα⁺ GCs.

(H) In vivo two-photon Ca²⁺ imaging of RFP⁺ (CaMKIIα⁺) and RFP⁻ GCs expressing GCaMP6s (green). Note the spontaneous Ca²⁺ events in RFP⁺ (CaMKIIα⁺) GCs, but not RFP⁻ GCs.

(I) GC activation under baseline conditions.

(J) Representative confocal images of cFos⁺ GCs (green) following CaMKIIα immunolabeling (top panel, red) and in CaMKIIα-tdTomato reporter mice (bottom panel, red). The arrows indicate CaMKIIα⁻ GCs. The arrowheads indicate CaMKIIα⁺ GCs.

(K) Quantification of the percentage of cFos/CaMKIIα⁺ and cFos⁺/tdTomato⁺ GCs.

Data are expressed as means ± SEM.

CaMKIIα⁻ GCs, the observed 15% difference in the percentage of responsive cells is likely an underestimation.

Our in vivo Ca²⁺ imaging was, however, restricted to the dorsal surface of the OB and allowed us only to determine the percentage of active GCs among virally infected CaMKIIα⁺ cells. Furthermore, it has previously been shown that GC activity in-creases with wakefulness [23]. We thus determined the percentage of CaMKIIα⁺ GCs among all activated cells throughout the GCL and whether their activation differed in awake animals. We performed immunolabeling for CaMKIIα and the immediate early gene *cFos*, a commonly used cell activity marker in the OB [26, 27]. We found that 77.2% ± 2.8% of the cFos⁺ GCs

located in the GCL were also CaMKIIα⁺ (Figures 2J and 2K). This result was confirmed in CaMKIIα-tdTomato reporter mice (Figures 2J and 2K). These findings extend our in vivo Ca²⁺ imaging results and suggest that CaMKIIα⁺ GCs are preferentially activated under baseline conditions throughout the GCL and in awake animals, and that, in addition to being biochemically heterogeneous, GCs in the adult OB are also functionally distinct.

The Population of CaMKIIα⁺ GCs Is Sensitive to Olfactory Experience

Given that CaMKIIα⁺ GCs are activated in the basal state, we next investigated the response of this subtype following an acute exposure to a novel odor or to sensory deprivation. We first performed in vivo two-photon Ca²⁺ imaging following the individual presentation of a set of six different odors. Odor stimulation resulted in a higher percentage of ON and OFF responsive cell-odor pairs in CaMKIIα⁺ RFP⁺/GCaMP6s⁺ GCs than in RFP⁻/GCaMP6s⁺ GCs (60.5% ± 3.0% for RFP⁺/GCaMP6s⁺ and 47.3% ± 4.7% for RFP⁻/GCaMP6s⁺ GCs; n = 414 and n = 1,522 cell-odor pairs from 6 mice; p < 0.05; Student's t test; Figures 3A–3D). We also observed differences in odor tuning (1.85 ± 0.16 and 1.2 ± 0.1 for RFP⁺/GCaMP6s⁺ GCs and RFP⁻/GCaMP6s⁺ GCs, respectively; p < 0.05; Kolmogorov-Smirnov test; Figure 3E), indicating once again that there are functional differences between these two GC subtypes. The peak amplitudes of responses (ΔF/F) were, however, not significantly different in RFP⁺/GCaMP6s⁺ and RFP⁻/GCaMP6s⁺ GCs (54.6% ± 2.3% and 37.0% ± 3.0%, respectively; Figure 3F). The temporal dynamics of odor responses in RFP⁺/GCaMP6s⁺ and RFP⁻/GCaMP6s⁺ GCs were also similar (Figure 3D). These data suggest that CaMKIIα⁺ GCs are more responsive to novel odor stimulations than their CaMKIIα⁻ counterparts.

To ascertain whether the increased responsiveness of CaMKIIα⁺ GCs to novel odors applies to the entire population of activated cells in the GCL, we immunolabeled for cFos and CaMKIIα following a 1-hr exposure of the mice to (+)-limonene and (−)-limonene. As expected, the odor exposure resulted in a significant increase in the total density of activated cFos⁺ GCs compared to unstimulated control mice (254,340 ± 25,652 cells/mm³ in controls versus 638,029 ± 79,083 cells/mm³ in odor-stimulated mice; p < 0.01; Figures 4A and 4B). This increase in the density of cFos⁺ GCs was not accompanied by statistically significant changes in the percentage of cFos⁺/CaMKIIα⁺ GCs (68.1% ± 6.3% in controls versus 80.8% ± 1.1% in odor-stimulated mice; Figure 4C). These results suggest that the presentation of a novel odor predominantly activates CaMKIIα⁺ GCs. The activation was the consequence of the recruitment of new CaMKIIα⁺ GCs rather than a shift from a CaMKIIα⁻ to a CaMKIIα⁺ subtype because no difference in the percentage of DAPI⁺/CaMKIIα⁺ GCs was observed (Figure 4D).

The specific activation of CaMKIIα⁺ GCs in the basal state and following the presentation of a novel odor indicated that this subtype is more sensitive to incoming sensory inputs. We thus hypothesized that blocking sensory inputs for 24 hr should decrease the percentage of cFos⁺/CaMKIIα⁺ GCs. Sensory deprivation decreased the density of activated cFos⁺ GCs (92,591 ± 4,832 cells/mm³ in the control OB versus 44,812 ± 3,443 cells/mm³ in the occluded OB; p < 0.01; Figures 4E and 4F) and reduced the percentage of cFos⁺/CaMKIIα⁺ GCs

(75.4% ± 1.3% in the control OB versus 59.0% ± 3.4% in the occluded OB; p < 0.05; Figure 4G). No change in the percentage of DAPI⁺/CaMKIIα⁺ GCs was observed (Figure 4H). These results suggest that CaMKIIα⁺ and CaMKIIα⁻ GCs are functionally distinct and that CaMKIIα⁺ GCs are more sensitive to incoming sensory inputs.

Structuro-functional Properties of CaMKIIα⁺ and CaMKIIα⁻ GCs

To shed light on the cellular mechanisms that underlie the distinct functional responses of CaMKIIα⁺ and CaMKIIα⁻ GCs, we next performed morphological and electrophysiological analyses of the two subtypes. We observed no differences in the length of the primary dendrites or the total dendritic arborization of GFP-expressing adult-born CaMKIIα⁺ and CaMKIIα⁻ GCs at 14, 21, and 28 days post-injection (dpi) (Figures 5A–5C). The spine densities on the distal dendrites of the two GC subtypes were also similar (Figure 5D). We next determined whether there were any morphological differences between early-born CaMKIIα⁺ and CaMKIIα⁻ GCs and again observed no differences in the length of the primary dendrites, total dendritic arborization, or spine density of the CaMKIIα⁺ and CaMKIIα⁻ GCs at 18 dpi (Figures 5A–5D).

We then determined whether CaMKIIα⁺ and CaMKIIα⁻ GCs had different electrophysiological properties. We used a CaMKIIα-GFP AAV to identify CaMKIIα⁺ GCs. For the control group, we used an AAV expressing a ubiquitous chicken β-actin (CBA) promoter. To assess the efficiency of these AAVs, we injected the RMS of adult C57BL/6 mice with one of the two AAVs. Two to three weeks post-infection, CaMKIIα immunolabeling of OB sections showed that 90.2% ± 4.1% of the GCs infected with the CaMKIIα-GFP AAV were CaMKIIα⁺ (n = 150 cells from 3 mice) whereas 53.2% ± 3.2% of the GFP⁺ GCs from the control animals injected with the CBA-GFP AAV were CaMKIIα⁺, which was expected given that the ubiquitous promoter targeted all GCs. Hence, any difference in electrophysiological properties observed using the two AAVs would be an underestimation given that the control group was composed of approximately 50% CaMKIIα⁺ GCs.

We recorded spontaneous excitatory postsynaptic currents (EPSCs) and inhibitory postsynaptic currents (IPSCs) from GCs to determine whether CaMKIIα⁺ GCs receive different excitatory and inhibitory inputs. No differences in the frequencies and amplitudes of spontaneous and miniature EPSCs (sEPSCs and mEPSCs) (Figures 5E–5G) or in the rise time, decay time, or charge of mEPSCs (Figure 5H) were observed. Recordings of spontaneous and miniature IPSCs (sIPSCs and mIPSCs) (Figures 5I and 5J) showed that the frequency of these events was the same for the two groups (Figure 5K). The amplitudes of the sIPSCs and mIPSCs were, however, significantly lower in CaMKIIα⁺ GCs (sIPSCs: 48.3 ± 5.2 pA for GCs [n = 11] versus 33.1 ± 2.9 pA for CaMKIIα⁺ GCs [n = 9], p < 0.05; mIPSCs: 27.6 ± 2.1 pA for GCs [n = 10] versus 21.7 ± 1.5 pA for CaMKIIα⁺ GCs [n = 8], p < 0.05; Figure 5L). We also observed that the rise and decay times of mIPSCs recorded from CaMKIIα⁺ GCs were faster than those recorded from the general population of GCs, which led to smaller charges for inhibitory events in CaMKIIα⁺ GCs (735 ± 63 pF for GCs [n = 10] versus 557 ± 29 pF for CaMKIIα⁺ GCs [n = 8]; p < 0.05; Figure 5M). These results
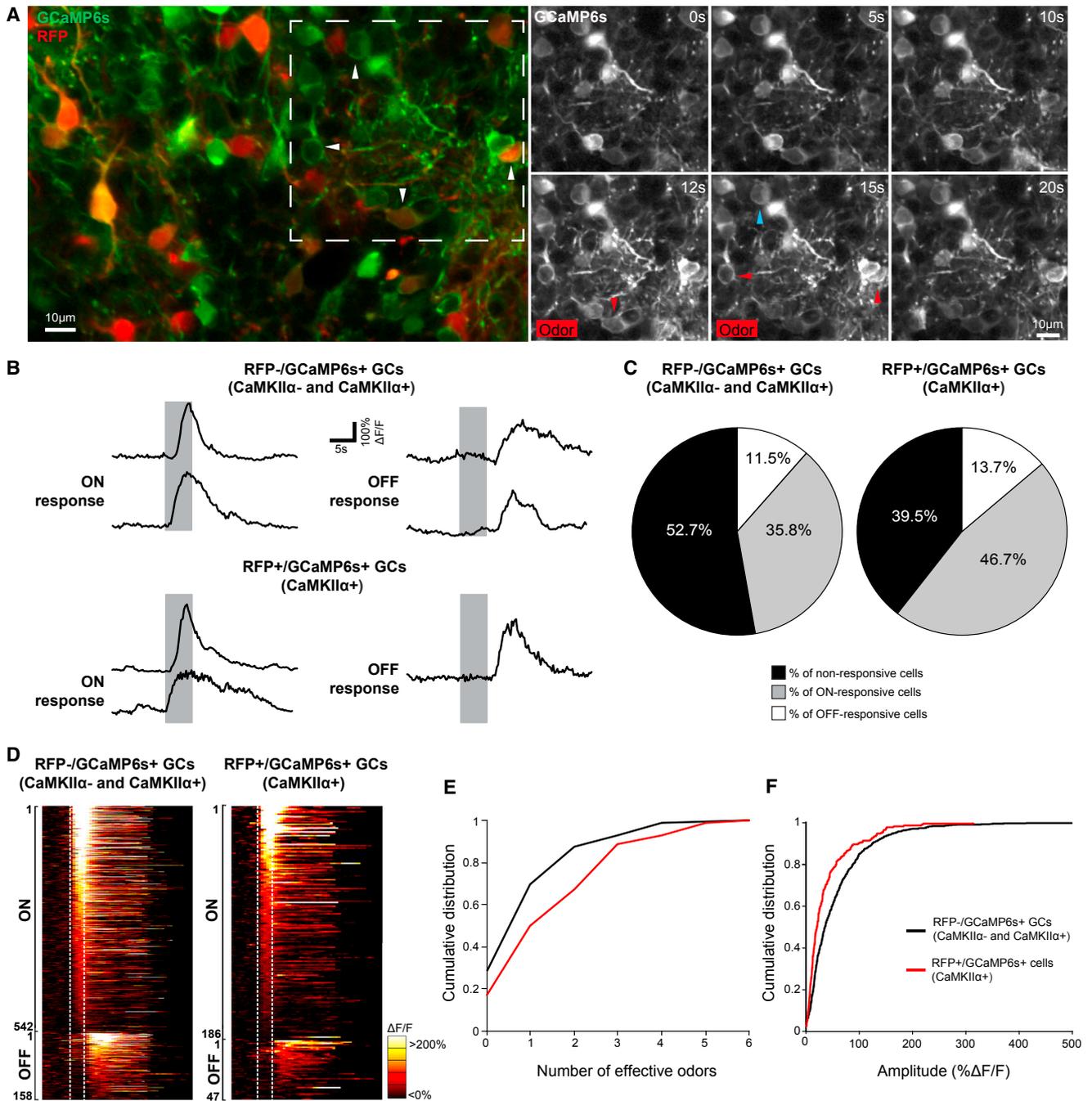
Figure 3. Sensory Stimulation Induces Higher Ca²⁺ Activity in CaMKIIα⁺ GCs

(A) In vivo two-photon Ca²⁺ imaging of RFP⁺/GCaMP6s⁺ (CaMKIIα⁺) and RFP⁻/GCaMP6s⁺ GCs following a 5-s odor stimulation with six structurally different odors. The odor-application interval is indicated in the lower left corner. Arrowheads indicate responsive (red) and non-responsive (blue) cells.

(B and C) Sample traces (B) and quantification (C) of ON- and OFF-responsive and non-responsive GCs for both populations. Odor application is indicated by the gray box.

(D) Pseudo-colored heatmaps of ON- and OFF-responsive GCs for RFP⁻/GCaMP6s⁺ and RFP⁺/GCaMP6s⁺ are shown. Cell odor pairs are sorted according to the amplitude of their responses.

(E and F) Cumulative distributions of odor tuning (E) and ΔF/F responses (F) of RFP⁻/GCaMP6s⁺ and RFP⁺/GCaMP6s⁺ (CaMKIIα⁺) GCs.

show that CaMKIIα⁺ GCs receive a lower level of inhibition, which may explain why they are preferentially activated in the basal state and following odor stimulation.

Perceptual Learning Activates CaMKIIα⁻ GCs

Because our in vivo Ca²⁺ imaging, electrophysiological, and early immediate gene expression results showed that the GC
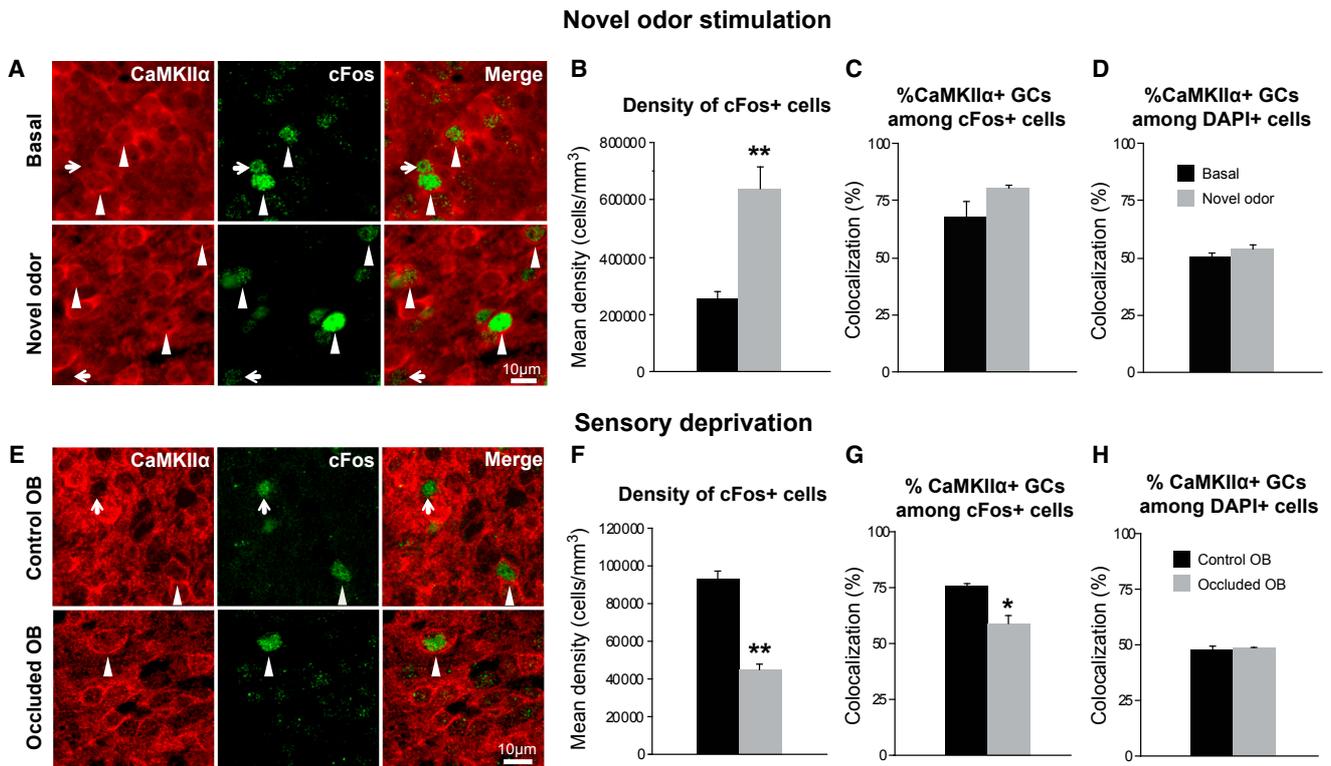
Figure 4. CaMKIIα⁺ Cells Are More Responsive to Sensory Activity

(A) Representative images of activated cFos⁺ GCs (green) also expressing CaMKIIα (red) in the basal state (top panel) and following an acute odor stimulation (bottom panel).

(B) The total density of cFos⁺ cells in the GCL increased after the acute odor exposure. **p < 0.01 Student's t test.

(C and D) Percentage of cFos⁺ (basal: n = 190 cells; acute exposure: n = 342 cells; n = 3 mice; C) and DAPI⁺ (basal: n = 1,940 cells; acute exposure: n = 2,012 cells; n = 3 mice; D) GCs co-expressing CaMKIIα in the basal state and following an acute odor stimulation.

(E–H) Effect of sensory deprivation on CaMKIIα⁺ GC activation. (E) CaMKIIα and cFos immunolabeling in control (top panel) and odor-deprived (bottom panel) OBs 24 hr after unilateral nostril occlusion is shown. The arrows and arrowheads indicate CaMKIIα⁻/cFos⁺ and CaMKIIα⁺/cFos⁺ GCs, respectively.

(F) Mean density of activated cFos⁺ GCs in the GCL of control and odor-deprived OBs is shown.

(G) The percentage of cFos⁺/CaMKIIα⁺ GCs was significantly lower in the occluded OB (gray) following the 24-hr sensory deprivation (control OB: n = 222 cells; occluded OB: n = 79 cells; n = 3 mice) is shown. *p < 0.05; **p < 0.01 paired Student's t test.

(H) Percentage of CaMKIIα⁺/DAPI⁺ (control OB: n = 616 cells; occluded OB: n = 560 cells; n = 3 mice) is shown.

Data are expressed as means ± SEM.

population is functionally heterogeneous, we wondered whether different GC subpopulations play different roles in distinct olfactory tasks. We first assessed the involvement of CaMKIIα⁺ and CaMKIIα⁻ GCs in perceptual learning, a non-associative form of odor learning that improves the ability of mice to discriminate between two perceptually similar odors following a passive 10-day exposure to the odors [27, 28]. The mice were submitted to odor enrichment with perceptually similar odorants ((+)-limonene and (−)-limonene) daily for 1 hr. The day after the end of the olfactory enrichment, the mice were separated into two groups, one of which was again submitted to the two odorants (learning + odor re-exposure group) for 1 hr, whereas the other group was not (learning group; Figure 6A). Re-exposing the animals to perceptually similar odors after the learning task resulted in an increase in cFos⁺ GC density (107,750 ± 7,750 cells/mm³ after re-exposure versus 78,500 ± 4,750 cells/mm³; n = 3; p < 0.001; Figures 6B and 6C). Interestingly, the perceptual learning task reduced the percentage of cFos⁺/CaMKIIα⁺ GCs from 77.2% ± 2.8% in the basal state to 49.0% ± 1% (n = 3; Fig-

ure 6D), indicating that CaMKIIα⁻ GCs are activated by this task. Re-exposing the animals to the odors after the perceptual learning task recruited CaMKIIα⁺ GCs (49.0% ± 1.1% of cFos⁺/CaMKIIα⁺ GCs for the learning group versus 62.0% ± 1.1% for the learning + odor re-exposure group; n = 3; p < 0.0001; Figure 6D). No change in the percentage of DAPI⁺/CaMKIIα⁺ cells was observed (Figure 6E). This suggests that olfactory perceptual learning relies on a broader recruitment of CaMKIIα⁻ GCs.

Nevertheless, these experiments did not rule out the involvement of CaMKIIα⁺ GCs in this odor-learning task. To address this issue, we inactivated CaMKIIα⁺ GCs in vivo using an AAV under the CaMKIIα promoter (CaMKIIα-HA-hM4D(Gi)-IRES-mCitrine) based on the DREADD approach [29]. The control mice were injected either with a CaMKIIα-GFP or a GFP under a synapsin (Syn) promoter AAV (Figure 6F). As expected, AAVs with the CaMKIIα promoter only infected the CaMKIIα⁺ GCs (87.3% ± 1.2% for the CaMKIIα-GFP AAV and 85.2% ± 1.9% for the CaMKIIα-DREADD AAV), whereas the Syn-GFP AAV
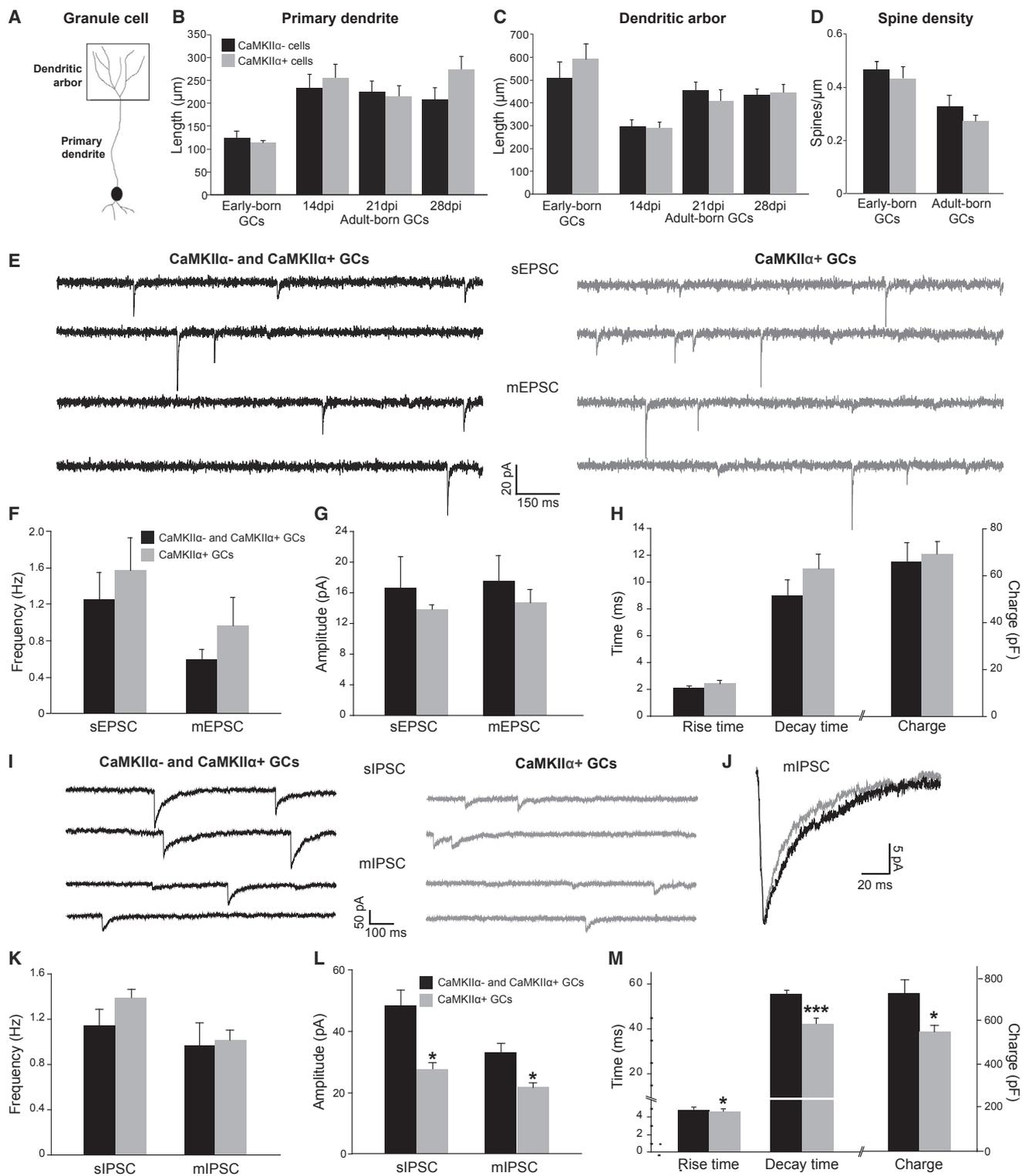
Figure 5. Morphological and Functional Characteristics of CaMKIIα⁺ and CaMKIIα⁻ GCs

(A) Schematic representation of GC morphology.

(B–D) Morphological analysis of early-born and adult-born CaMKIIα⁺ and CaMKIIα⁻ GCs. The lengths of the primary dendrites (B), dendritic arborizations (C), and spine densities (D) were similar for both GC subtypes.

(E) sEPSCs and mEPSCs were recorded from CaMKIIα-GFP (gray traces) and CBA-GFP (black traces) AAV-infected GCs.

(legend continued on next page)

infected both subtypes of GCs. To test the efficiency of our pharmacogenetic approach, we administrated CNO, the DREADD-receptor ligand, to both groups of mice and perfused the animals 90 min later. Immunolabeling for cFos and GFP showed that CaMKIIα-DREADD AAV-injected mice contained significantly fewer GFP$^+$/cFos$^+$ GCs (29.0% ± 2.0% in CaMKIIα-GFP-infected GCs versus 16.0% ± 1.6% in CaMKIIα-DREADD-infected GCs; n = 3 mice; p < 0.05; Figure 6G). Similarly, Syn-DREADD (Syn-HA-hM4D(Gi)-mCherry) AAV-infected GCs contained significantly fewer mCherry$^+$/cFos$^+$ GCs than Syn-GFP-infected GCs (16.8% ± 2.5% in Syn-GFP-infected GCs versus 3.3% ± 1.7% in Syn-DREADD-infected GCs; n = 3 mice; p < 0.01; Figure 6H). We next determined whether the inhibition of CaMKIIα$^+$ GCs during the learning task (Figure 6I) affected the discrimination of perceptually similar odors. As reported previously [27, 28], the mice were able to discriminate between two perceptually close odorants after the learning task (post-enrichment test: 162.9% ± 27.7% increase in exploration time for the dishabituation odor versus 100.0% ± 17.2% for the habituation odor; n = 18 mice; p < 0.05), but not before (pre-enrichment test: 75.5% ± 14.9% increase for the dishabituation odor versus 100.0% ± 17.6% for the habituation odor; n = 18 mice; p = 0.2; Figure 6J). Interestingly, the inhibition of CaMKIIα$^+$ GCs during the learning task did not affect the ability of these mice to discriminate between two perceptually similar odors (post-enrichment test: 185.5% ± 61.1% increase for the dishabituation odor versus 100.0% ± 36.8% for the habituation odor; n = 7 mice; p < 0.05; Figure 6K). The unaltered perceptual learning following the pharmacogenetic inhibition of CaMKIIα$^+$ GCs may be simply due to the fact that GCs in general are not needed for this type of learning. To test this possibility, we inactivated GCs in a subtype-independent manner using DREADDs under the Syn promoter. This subtype-independent inhibition of GCs during the learning task affected the ability of mice to discriminate between two perceptually similar odors (post-enrichment test: 82.1% ± 32.4% for the dishabituation odor versus 100.0% ± 25.3% for the habituation odor; n = 10 mice; Figure 6L). These results suggest that, whereas GCs are required for perceptual learning, CaMKIIα$^+$ GCs are not involved in this type of learning, indicating that CaMKIIα$^-$ GCs are required for perceptual learning.

CaMKIIα$^+$ GCs Are Essential for Spontaneous and Go/No-Go Odor Discrimination

We next determined whether CaMKIIα$^+$ GCs are involved in other odor discrimination paradigms that, unlike perceptual learning, are based on active odor learning (go/no-go odor discrimination and long-term odor-associative memory) or spontaneous habituation/dishabituation tasks. In the long-term associative memory task (Figure S1A), mice were conditioned to associate one

of two chemically similar odors ((+)-carvone) with a sugar reward. We used pseudo-conditioned mice, which received the reward independently of the odor presented ((+)-carvone or (−)-carvone) as a control. During the test, the mice were re-exposed to the two odors, and the exploration time was measured 24 hr after a 4-day training period. The conditioned mice spent significantly more time exploring the reward-associated odor, whereas the pseudo-conditioned mice spent the same amount of time investigating both enantiomers (Figure S1B). The density of activated cFos$^+$ cells, the percentage of DAPI$^+$ cells expressing CaMKIIα, and the percentage of cFos$^+$/CaMKIIα$^+$ GCs were similar for the conditioned and pseudo-conditioned groups (Figures S1C and S1F).

We next used the go/no-go operant-conditioning paradigm, in which mice are trained to insert their snouts into the odor-sampling port of an olfactometer and to associate a specific odor (0.1% octanal; S+) with a water reward. The mice were able to reach the criterion of 80% correct responses in a few blocks of 20 odor presentation trials. The control group was subjected to the same go/no-go procedure but received the water reward independently of the odor used (S+ or S−). An analysis of the phenotypes of the GCs activated following this task did not reveal any difference in the density of cFos$^+$ GCs (Figures 7A and 7B), the percentage of CaMKIIα$^+$/cFos$^+$ GCs (Figure 7C), or the percentage of CaMKIIα$^+$/DAPI$^+$ GCs (Figure 7D).

The lack of difference in the percentage of activated CaMKIIα$^+$ GCs following the long-term associative memory and go/no-go odor-discrimination learning tasks may reflect the high activation level of this subtype in the basal state. We thus used a pharmacogenetic approach to selectively inhibit CaMKIIα$^+$ GCs (Figure 7E) and to determine their contribution to the go/no-go odor-discrimination task. This made it possible to precisely administer structurally distinct odors as well as complex odor mixtures. The mice injected with both CaMKIIα-GFP and CaMKIIα-DREADDs AAVs were able to discriminate between two structurally distinct odors (0.1% octanal versus 0.1% decanal) following the application of CNO (Figure 7F). However, pharmacogenetic inactivation of CaMKIIα$^+$ GCs affected the ability of the mice to discriminate between complex odor mixtures (0.6% (+)-carvone/0.4% (−)-carvone versus 0.4% (+)-carvone/0.6% (−)-carvone; Figure 7G). The mice whose CaMKIIα$^+$ GCs were pharmacogenetically inactivated required more blocks to reach the criterion of 80% correct responses (13.1 ± 1.7 blocks for control mice versus 20.8 ± 1.3 blocks for mice in the experimental group; n = 7 and 8 mice, respectively; p < 0.01; Figure 7G). These results indicate that CaMKIIα$^+$ GCs are required for go/no-go odor discrimination learning of complex odor mixtures.

We next used a spontaneous habituation/dishabituation odor-discrimination task in which the mice were first habituated to

---

(F–H) The frequencies (F) and amplitudes (G) of sEPSCs and mEPSCs, as well as the rise times, decay times, and charges (H) of mEPSCs from the two GC populations were indistinguishable. sEPSCs: GCs (n = 9), CaMKIIα$^+$ GCs (n = 7); mEPSCs: GCs (n = 7), CaMKIIα$^+$ GCs (n = 7).
(I) Examples of sIPSCs and mIPSCs recorded from CaMKIIα-GFP- (gray traces) or CBA-GFP- (black traces) infected GCs.
(J) Scaled mIPSCs recorded in a CaMKIIα$^+$ GC (gray trace) and the general population of GCs (black trace).
(K and L) The frequencies of the sIPSCs and mIPSCs of the two GC populations were the same (K), whereas the amplitude was significantly lower in CaMKIIα$^+$ GCs (L).
(M) The rise times, decay times, and charges of mIPSCs from CaMKIIα$^+$ GCs were also significantly different from those from the general population of GCs. sIPSCs: n = 11 GCs, CaMKIIα$^+$ GCs (n = 9); mIPSCs: GCs (n = 10), CaMKIIα$^+$ GCs (n = 8); *p < 0.05; ***p < 0.001 Student's t test.
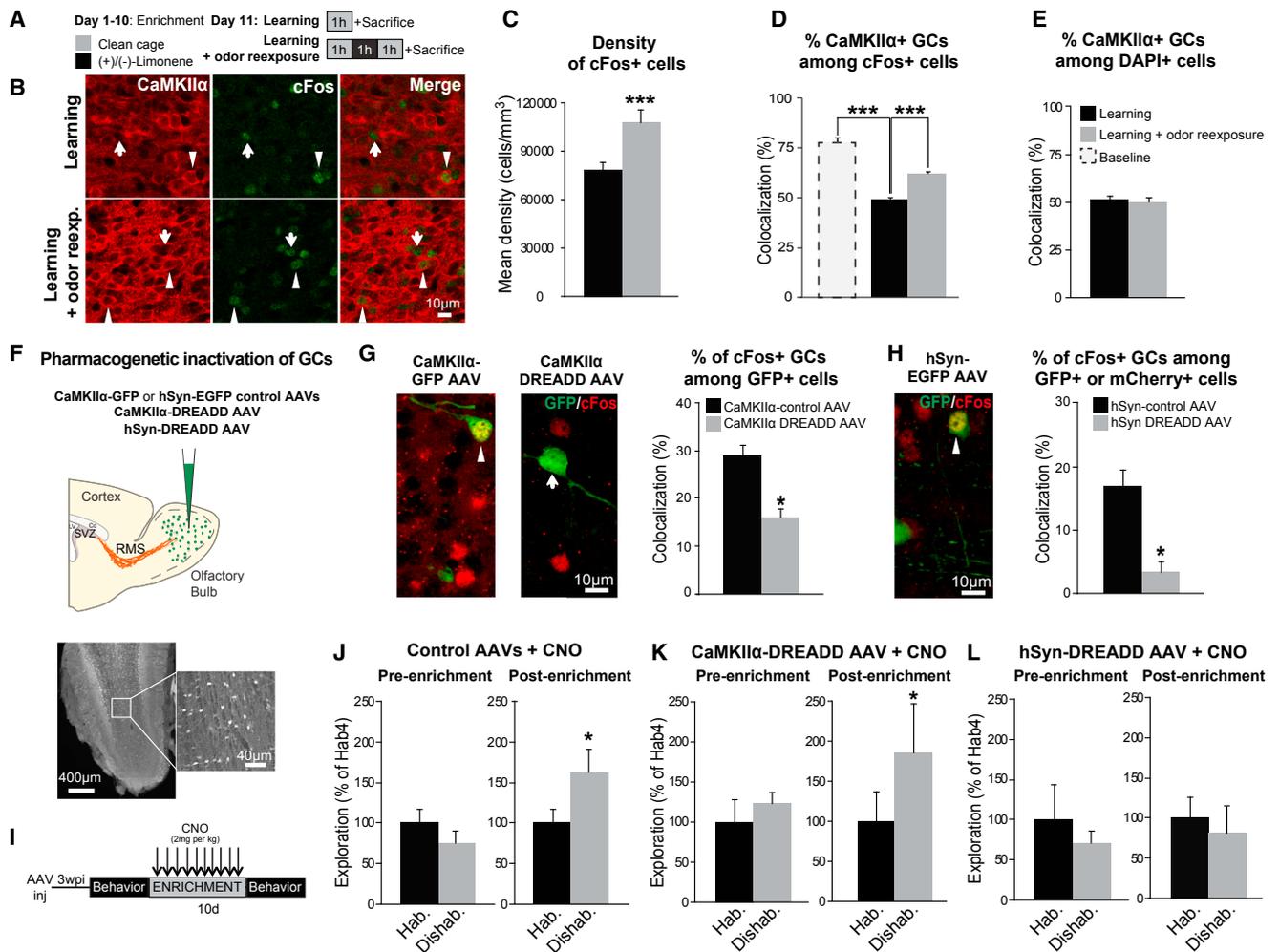Data are expressed as means ± SEM.

Figure 6. CaMKIIα+ GCs Are Not Required for Perceptual Learning

(A) Experimental procedure for the perceptual learning task.

(B) Representative images of cFos and CaMKIIα immunolabeling after learning (learning) and learning followed by odor re-exposure (learning + odor re-exposure).

(C) Density of cFos+ cells following the perceptual learning task.

(D) Percentage of cFos+/CaMKIIα+ GCs following the perceptual learning task. For comparison purposes, the percentage of cFos+/CaMKIIα+ GCs observed in baseline conditions (Figure 2K) is plotted (dashed bar).

(E) Percentage of DAPI+/CaMKIIα+ GCs.

(F) Schematic representation and photomicrograph of AAV injections in the OB to pharmacogenetically modulate GC subtypes activity.

(G) Confocal images of coronal OB sections and quantification of GFP+/cFos+ GCs following CNO injection. Representative images of GCL injected with a control (left panel) or a CaMKIIα-DREADD-expressing AAV (right panel), labeled with GFP, are shown. *p < 0.05 paired Student's t test.

(H) Confocal image and quantification of GFP+/cFos+ in Syn-GFP and mCherry+/cFos+ in Syn-DREADD GCs following CNO injection. *p < 0.05 Student's t test.

(I) Experimental protocol used to inactivate GCs during the perceptual learning task.

(J–L) Mean exploration time, expressed as the percentage of increase during the presentations of dishabituation versus habituation odors, of control CaMKIIα-GFP or Syn-GFP AAV (J), CaMKIIα-DREADD (K), and Syn-DREADD (L) AAV-injected mice before and 10 days after the enrichment period. *p < 0.05 paired Student's t test. n = 18, 7, and 10 mice for the control, CaMKIIα-DREADD, and Syn-DREADD groups, respectively.

Data are expressed as means ± SEM.

(+)-carvone by four consecutive presentations followed by the presentation of a new (dishabituation) odor ((−)-carvone; Figure 7H). For the control group, the mice were presented with the same habituation odor during the last odor presentation (habituation/habituation group; Figure 7H). As expected, the mice from the two groups became habituated to the first odor. The increase in exploration time observed with the experimental habituation/dishabituation group when the second odor was presented showed that the mice were able to spontaneously discriminate between the two odorants (143.7% ± 24.0% increase in dishabituation odor compared to the last presentation of the habituation odor; n = 11; p < 0.05; Figure 7I). An analysis of the phenotypes of the GCs activated following the odor-discrimination task did not reveal any differences in the density of cFos+ GCs, the percentage of CaMKIIα+/DAPI+ GCs, or the percentage of CaMKIIα+/cFos+ GCs (n = 4 mice per group; Figures 7J–7M).

Go/no-go operant conditioning

A CaMKIIα | cFos | Merge

Control

Go/no-go

10μm

B Density of cFos+ cells

C % CaMKIIα+ GCs among cFos+ cells

D % CaMKIIα+ GCs among DAPI+ cells

- Control
- Go/no-go

E Pharmacogenetic inactivation of CaMKIIα GCs

CNO (2mg per kg)

AAV injection 3wpi 30' Go/no-go

S+ → lick (hit) / reject (error)
S- → lick (error) / reject (hit)

F Structurally different odors (S+ Octanal vs S- Decanal)

- CaMKIIα control AAV
- CaMKIIα DREADD AAV

Chance level

Blocks to criterion

G Odor mixture (S+ 60% (+)-Carvone / 40% (-)-Carvone vs S- 40% (+)-Carvone / 60% (-)-Carvone)

Chance level

Blocks to criterion **

Spontaneous odor discrimination

H Control habituation group

O1 5' 20' O2 H1 H2 H3 H4 H5 1h → Sacrifice

Experimental habituation/dishabituation group

O1 5' 20' O2 H1 H2 H3 H4 D 1h → Sacrifice

- Mineral oil
- Habituation : (+)-Carvone
- Dishabituation : (-)-Carvone

I Habit./habit. | Habit./dishabit.

Hab.4 Hab.5 | Hab.4 Dishab. *

J CaMKIIα | cFos | Merge

Habit./habit.

Habit./dishabit.

10μm

K Density of cFos+ cells

L % CaMKIIα+ GCs among cFos+ cells

M % CaMKIIα+ GCs among DAPI+ cells

- Habit/habit.
- Habit./dishabit.

N Pharmacogenetic inactivation of CaMKIIα GCs

CNO (2mg per kg)

O1 5' 20' O2 H1 H2 H3 H4 30' D

- Mineral oil
- Habituation : (+)-Carvone
- Dishabituation : (-)-Carvone

O Control AAV + CNO

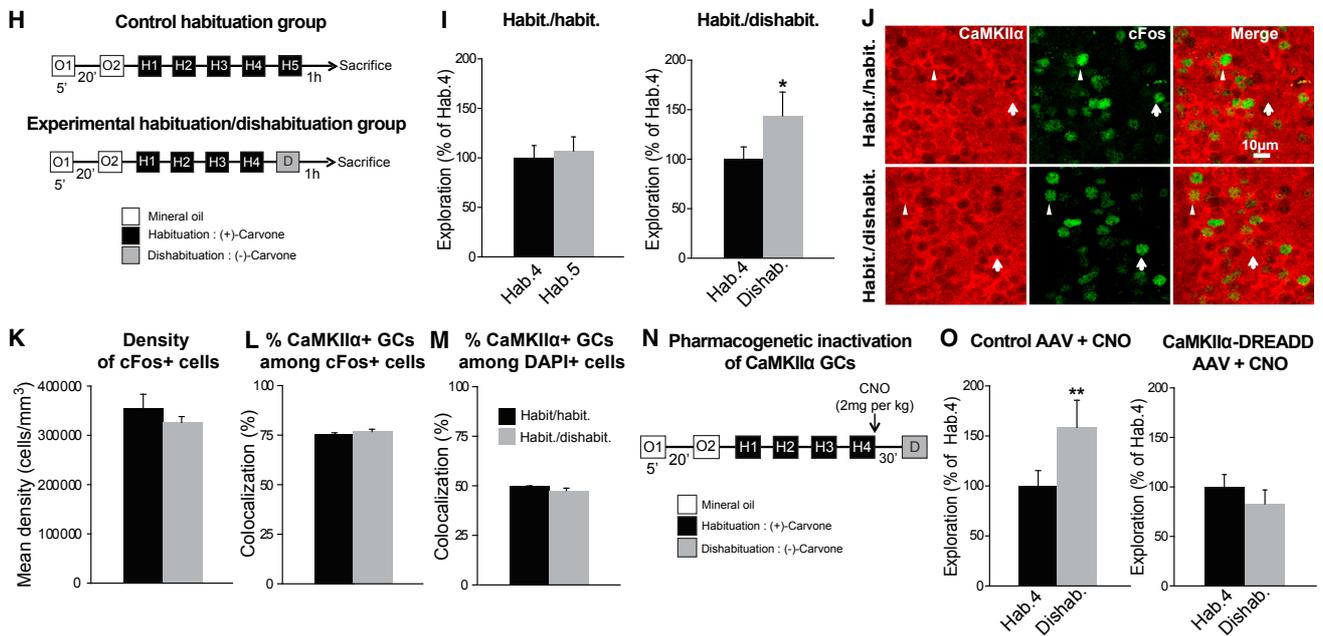Hab.4 Dishab. **

CaMKIIα-DREADD AAV + CNO

Hab.4 Dishab.

Figure 7. CaMKIIα⁺ GCs Are Required for Go/No-Go Odor Discrimination Learning and Spontaneous Odor Discrimination

(A) CaMKIIα (red) and cFos (green) immunolabeling in the control (top panel) and experimental (bottom panel) groups following a go/no-go odor discrimination task. The arrows and arrowheads indicate CaMKIIα⁻ and CaMKIIα⁺ GCs, respectively.

(B) The density of cFos-immunolabeled cells did not change following the go/no-go task (n = 3 mice per group).

(C) Percentage of cFos⁺/CaMKIIα⁺ cells (n = 847 and 766 cells from 3 mice for the control and experimental groups, respectively).

(D) Percentage of CaMKIIα⁺/DAPI⁺ GCs (n = 4,500 and 5,278 cells from 3 mice for control and experimental groups, respectively).

(E) Experimental design for the pharmacogenetic inhibition of CaMKIIα⁺ GCs during the go/no-go odor discrimination task.

(F and G) Pharmacogenetic inhibition of CaMKIIα⁺ GCs affected complex odor mixture discrimination (G) but spared that of structurally distinct odors (F). $**p < 0.01$; Student's t test. n = 7 and 8 mice for the control and CaMKIIα-DREADD groups, respectively.

(H) Schematic representation of the spontaneous odor-discrimination task.

(legend continued on next page)

As for long-term associative odor memory and go/no-go odor-discrimination learning, we reasoned that the lack of difference in the percentage of activated CaMKIIα$^+$ GCs reflects their high activation level in the basal state. We thus again used a pharmacogenetic approach to selectively inhibit CaMKIIα$^+$ GCs and to determine their contribution to spontaneous odor discrimination (Figure 7N). Whereas the mice injected with the control CaMKIIα-GFP AAV were able to discriminate between the two enantiomers (158.6% ± 27.1% increase in dishabituation odor compared to the last presentation of the habituation odor; n = 9; p < 0.01; Figure 7O), the inhibition of the CaMKIIα$^+$ GCs disrupted the mice's ability to discriminate between two similar odors (82.9% ± 14.0% compared to the last presentation of the habituation odor; n = 10; p = 0.3; Figure 7O). These results indicate that CaMKIIα$^+$ GCs in the adult OB are also required for spontaneous odor discrimination of similar odors.

DISCUSSION

We showed that there are two functionally distinct subtypes of GC in the OB that fulfill different roles in odor behavior. CaMKIIα$^+$ GCs receive weaker inhibitory inputs, making them more susceptible to activation by olfactory stimuli. This subtype of GC is essential for go/no-go operant conditioning and habituation/dishabituation spontaneous odor discrimination, but not for perceptual learning. On the other hand, CaMKIIα$^-$ GCs are preferentially activated by and are involved in perceptual learning.

One challenge in comprehending odor information processing is understanding the role played by different cell types in the OB. Despite the fact that GCs make up the largest neuronal population in the OB with neurochemically distinct subtypes, little is known about their functional heterogeneity. Studies aimed at addressing their roles in sensory information processing and odor behavior have usually considered them as a homogeneous population of interneurons [4, 5, 18]. Using in vivo two-photon imaging of GCaMP6s-infected GCs, we identified two types of GCs based on their level of spontaneous activity and their responses to odor stimulation. We showed that GCs are heterogeneous and that a substantial proportion of them are already active under basal conditions and following odor stimulation. Our study revealed the molecular and cellular mechanisms underlying these heterogeneous responses. In fact, 60%–70% of responsive cells belonged to the CaMKIIα$^+$ GC subtype that receives a lower level of inhibition than their CaMKIIα$^-$ counterparts. It should be noted, however, that the electrophysiological recordings were performed with adult-born GC populations, and it remains to be shown whether the

same differences in the level of inhibition exist in early-born CaMKIIα$^+$ and CaMKIIα$^-$ GCs. Our in vivo Ca^{2+} imaging data were corroborated by the early immediate gene analysis showing that the vast majority (70%–90%) of cFos$^+$ GCs activated in basal conditions or following go/no-go operant conditioning, long-term associative memory, and spontaneous habituation/dishabituation odor discrimination tasks belong to the CaMKIIα$^+$ subtype. In contrast, perceptual learning recruited CaMKIIα$^-$ GCs, indicating that these two subtypes of GCs may be differently modulated during distinct olfactory tasks. CaMKIIα$^+$ GCs receive weaker inhibitory inputs and are more prone to activation by sensory stimuli whereas CaMKIIα$^-$ GCs receive stronger inhibitory inputs and require stronger excitatory stimuli to be recruited during particular olfactory tasks. This may occur in perceptual learning tasks that rely on stronger sensory stimuli (1 hr/day exposure to undiluted odors for 10 days). Our pharmacogenetic experiments indicate that GC subtypes are not only differently modulated but also play diverse roles in distinct olfactory tasks.

We showed that the CaMKIIα$^+$ and CaMKIIα$^-$ GC subtypes fulfill distinct functional roles in odor information processing. However, other GC subtypes have been identified based on the expression of neurochemical markers, such as calretinin, 5T4, neurogranin, and mGluR2 [7–9, 30, 31]. The roles of 5T4-expressing GCs in odor detection and discrimination have recently been described [32], whereas the roles of other GC subtypes in odor behavior remain to be determined. The adult OB also constantly receives new neurons that add another level of complexity to deciphering the roles of specific GC subtypes in odor-information processing. Many studies have shown that adult-born neurons are involved in different types of odor behavior, including short- and long-term odor memory, odor discrimination, and maternal and social behaviors [18–20, 33–36]. Whereas these studies have provided new insights into the roles of adult-born neurons in the functioning of the OB neuronal network and the execution of selected olfactory behaviors, we [20, 33] and others [18, 19, 34, 36] have considered adult-born GCs as a homogeneous population of cells. However, the results presented here indicate that adult-born GCs are a functionally heterogeneous population of interneurons with distinct electrophysiological properties. This, in turn, implies that, like early-born neurons, the roles of these distinct subtypes of adult-born cells in the functioning of the OB network and odor behavior may be quite different, depending on the level of their activation by a given behavioral task and their roles in the OB network.

CaMKIIα is one of the most abundant proteins in the brain, making up 1% or 2% of the total protein content, with the

(I) Mean exploration time of mice in the experimental and control groups exposed to either a new dishabituation odor or the same habituation odor, respectively (n = 11 and 8 mice, respectively). *p < 0.05; paired Student's t test.
(J) Confocal images of cFos- and CaMKIIα-immunolabeled GCs in the control habituation (top panel) and experimental habituation/dishabituation groups (bottom panel). The arrows and arrowheads indicate CaMKIIα$^-$ and CaMKIIα$^+$ GCs, respectively.
(K) The density of cFos-immunolabeled cells did not change following the discrimination task (n = 4 mice per group).
(L) Percentage of cFos$^+$/CaMKIIα$^+$ cells in the two groups (n = 484 and 587 cells from 4 mice for the habituation and habituation/dishabituation groups, respectively).
(M) Percentage of CaMKIIα$^+$/DAPI$^+$ GCs (n = 891 and 1,035 cells from 4 mice from the habituation and habituation/dishabituation groups, respectively).
(N) Experimental protocol for the pharmacogenetic inhibition of CaMKIIα$^+$ GCs during the odor-discrimination task.
(O) Whereas administering CNO to control CaMKIIα-GFP mice did not affect discrimination (left histogram), administering CNO resulted in a complete block of odor discrimination in CaMKIIα-DREADD mice (right histogram). **p < 0.01 paired Student's t test. n = 9 and 10 mice for the control and CaMKIIα-DREADD groups, respectively.
Data are expressed as means ± SEM. See also Figure S1.

α subunit being the most prominent in the brain [37]. CaMKIIα expression is usually confined to excitatory neurons [38, 39], but principal cells in the OB lack this enzyme, which is specifically expressed by GCs [10, 11]. Our finding that CaMKIIα$^+$ GCs receive weaker inhibitory inputs than their CaMKIIα$^-$ counterparts raises an important question as to whether CaMKIIα confers a GC subtype with functional properties distinct from other interneurons. Whereas this question requires further investigation, it is interesting to note that CaMKIIα is a major player in the synaptic development and plasticity of both excitatory and inhibitory synapses. Indeed, CaMKIIα plays an essential role in decoding Ca^{2+} signals in excitatory neurons and modulates the synaptic remodeling and plasticity of these cells [40–43]. CaMKIIα is also involved in the remodeling and plasticity of inhibitory synapses via trafficking of different GABA$_A$ receptor subunits as well as gephyrin, the main scaffolding protein of inhibitory synapses [44–47]. Several GABA$_A$ receptor subunits are highly expressed in the OB [48], and differences in subunit composition determine the functional characteristics of GABA$_A$ receptors [49]. Differences in the amplitudes and kinetics of the inhibitory currents of the two GC subtypes may thus result from a differential expression of GABA$_A$ receptor subunits. It is also possible that different GC subtypes receive inhibitory inputs originating from distinct sources that confer different functions. A number of local and long-ranging GC-inhibitory inputs have been identified [1, 50, 51], but it is not known whether they segregate differently onto distinct GC subtypes. Altogether, our results provide evidence for the existence of functionally distinct GC subtypes in the adult OB and show that they each have a distinct involvement in odor behavior.

STAR★METHODS

Detailed methods are provided in the online version of this paper and include the following:

- KEY RESOURCES TABLE
- CONTACT FOR REAGENT AND RESOURCE SHARING
- EXPERIMENTAL MODEL AND SUBJECT DETAILS
- METHOD DETAILS
  - Stereotaxic injections
  - Cranial window surgery and in vivo two-photon calcium imaging
  - Immunohistochemistry
  - Morphological analysis
  - Electrophysiological recordings
  - Novel odor stimulation
  - Sensory deprivation
  - Behavioral procedures
  - Perceptual learning
  - Long-term associative memory
  - Pharmacogenetic inactivation of CaMKIIα$^+$ GCs
- QUANTIFICATION AND STATISTICAL ANALYSIS
- DATA AND SOFTWARE AVAILABILITY

SUPPLEMENTAL INFORMATION

Supplemental Information includes one figure and two movies and can be found with this article online at https://doi.org/10.1016/j.cub.2017.09.058.

AUTHOR CONTRIBUTIONS

S.M., A.T., I.C., and A.S. designed the study. S.M., S.G., L.S.D., L.D., and D.H. performed the experiments and analyzed the data. Z.C. and M.H. provided the CaMKIIα-tdTomato mice. D.C. provided the custom two-photon imaging system. S.L. and P.D.K. provided the MATLAB script for the Ca^{2+} imaging analyses. M.-A.L.-C. wrote the MATLAB script for the tuning analysis. S.M. and A.S. wrote the manuscript, taking into consideration the comments of the other authors.

REFERENCES

1. Shepherd, G.M., Chen, W.R., and Greer, C.A. (2004). Olfactory bulb. In The Synaptic Organization of the Brain, G.M. Shepherd, ed. (Oxford University Press), pp. 165–216.

2. Fukunaga, I., Herb, J.T., Kollo, M., Boyden, E.S., and Schaefer, A.T. (2014). Independent control of gamma and theta activity by distinct interneuron networks in the olfactory bulb. Nat. Neurosci. *17*, 1208–1216.

3. Urban, N.N. (2002). Lateral inhibition in the olfactory bulb and in olfaction. Physiol. Behav. *77*, 607–612.

4. Gschwend, O., Abraham, N.M., Lagier, S., Begnaud, F., Rodriguez, I., and Carleton, A. (2015). Neuronal pattern separation in the olfactory bulb improves odor discrimination learning. Nat. Neurosci. *18*, 1474–1482.

5. Nunes, D., and Kuner, T. (2015). Disinhibition of olfactory bulb granule cells accelerates odour discrimination in mice. Nat. Commun. *6*, 8950.

6. Wienisch, M., and Murthy, V.N. (2016). Population imaging at subcellular resolution supports specific and local inhibition by granule cells in the olfactory bulb. Sci. Rep. *6*, 29308.

7. Batista-Brito, R., Close, J., Machold, R., and Fishell, G. (2008). The distinct temporal origins of olfactory bulb interneuron subtypes. J. Neurosci. *28*, 3966–3975.

8. Gribaudo, S., Bovetti, S., Garzotto, D., Fasolo, A., and De Marchis, S. (2009). Expression and localization of the calmodulin-binding protein neurogranin in the adult mouse olfactory bulb. J. Comp. Neurol. *517*, 683–694.

9. Imamura, F., Nagao, H., Naritsuka, H., Murata, Y., Taniguchi, H., and Mori, K. (2006). A leucine-rich repeat membrane protein, 5T4, is expressed by a subtype of granule cells with dendritic arbors in specific strata of the mouse olfactory bulb. J. Comp. Neurol. *495*, 754–768.

10. Néant-Fery, M., Pérès, E., Nasrallah, C., Kessner, M., Gribaudo, S., Greer, C., Didier, A., Trembleau, A., and Caillé, I. (2012). A role for dendritic translation of CaMKIIα mRNA in olfactory plasticity. PLoS ONE *7*, e40133.

11. Zou, D.-J., Greer, C.A., and Firestein, S. (2002). Expression pattern of alpha CaMKII in the mouse main olfactory bulb. J. Comp. Neurol. *443*, 226–236.

12. Chaker, Z., Aïd, S., Berry, H., and Holzenberger, M. (2015). Suppression of IGF-I signals in neural stem cells enhances neurogenesis and olfactory function during aging. Aging Cell *14*, 847–856.

13. Lagace, D.C., Whitman, M.C., Noonan, M.A., Ables, J.L., DeCarolis, N.A., Arguello, A.A., Donovan, M.H., Fischer, S.J., Farnbauch, L.A., Beech, R.D., et al. (2007). Dynamic contribution of nestin-expressing stem cells to adult neurogenesis. J. Neurosci. *27*, 12623–12629.

14. Ninkovic, J., Mori, T., and Götz, M. (2007). Distinct modes of neuron addition in adult mouse neurogenesis. J. Neurosci. *27*, 10906–10911.

15. Gengatharan, A., Bammann, R.R., and Saghatelyan, A. (2016). The role of astrocytes in the generation, migration, and integration of new neurons in the adult olfactory bulb. Front. Neurosci. *10*, 149.

16. Ihrie, R.A., and Alvarez-Buylla, A. (2011). Lake-front property: a unique germinal niche by the lateral ventricles of the adult brain. Neuron *70*, 674–686.

17. Lepousez, G., Nissant, A., and Lledo, P.-M. (2015). Adult neurogenesis and the future of the rejuvenating brain circuits. Neuron *86*, 387–401.

18. Alonso, M., Lepousez, G., Sebastien, W., Bardy, C., Gabellec, M.-M., Torquet, N., and Lledo, P.-M. (2012). Activation of adult-born neurons facilitates learning and memory. Nat. Neurosci. *15*, 897–904.

19. Arruda-Carvalho, M., Akers, K.G., Guskjolen, A., Sakaguchi, M., Josselyn, S.A., and Frankland, P.W. (2014). Posttraining ablation of adult-generated olfactory granule cells degrades odor-reward memories. J. Neurosci. *34*, 15793–15803.

20. Breton-Provencher, V., Lemasson, M., Peralta, M.R., 3rd, and Saghatelyan, A. (2009). Interneurons produced in adulthood are required for the normal functioning of the olfactory bulb network and for the execution of selected olfactory behaviors. J. Neurosci. *29*, 15245–15257.

21. Imayoshi, I., Sakamoto, M., Ohtsuka, T., Takao, K., Miyakawa, T., Yamaguchi, M., Mori, K., Ikeda, T., Itohara, S., and Kageyama, R. (2008). Roles of continuous neurogenesis in the structural and functional integrity of the adult forebrain. Nat. Neurosci. *11*, 1153–1161.

22. Malvaut, S., and Saghatelyan, A. (2016). The role of adult-born neurons in the constantly changing olfactory bulb network. Neural Plast. *2016*, 1614329.

23. Kato, H.K., Chu, M.W., Isaacson, J.S., and Komiyama, T. (2012). Dynamic sensory representations in the olfactory bulb: modulation by wakefulness and experience. Neuron *76*, 962–975.

24. Breton-Provencher, V., Bakhshetyan, K., Hardy, D., Bammann, R.R., Cavarretta, F., Snapyan, M., Côté, D., Migliore, M., and Saghatelyan, A. (2016). Principal cell activity induces spine relocation of adult-born interneurons in the olfactory bulb. Nat. Commun. *7*, 12659.

25. Livneh, Y., Feinstein, N., Klein, M., and Mizrahi, A. (2009). Sensory input enhances synaptogenesis of adult-born neurons. J. Neurosci. *29*, 86–97.

26. Inaki, K., Takahashi, Y.K., Nagayama, S., and Mori, K. (2002). Molecular-feature domains with posterodorsal-anteroventral polarity in the symmetrical sensory maps of the mouse olfactory bulb: mapping of odourant-induced Zif268 expression. Eur. J. Neurosci. *15*, 1563–1574.

27. Mandairon, N., Didier, A., and Linster, C. (2008). Odor enrichment increases interneurons responsiveness in spatially defined regions of the olfactory bulb correlated with perception. Neurobiol. Learn. Mem. *90*, 178–184.

28. Daroles, L., Gribaudo, S., Doulazmi, M., Scotto-Lomassese, S., Dubacq, C., Mandairon, N., Greer, C.A., Didier, A., Trembleau, A., and Caillé, I. (2016). Fragile X mental retardation protein and dendritic local translation of the alpha subunit of the calcium/calmodulin-dependent kinase II messenger RNA are required for the structural plasticity underlying olfactory learning. Biol. Psychiatry *80*, 149–159.

29. Roth, B.L. (2016). DREADDs for neuroscientists. Neuron *89*, 683–694.

30. Merkle, F.T., Fuentealba, L.C., Sanders, T.A., Magno, L., Kessaris, N., and Alvarez-Buylla, A. (2014). Adult neural stem cells in distinct microdomains generate previously unknown interneuron types. Nat. Neurosci. *17*, 207–214.

31. Murata, K., Imai, M., Nakanishi, S., Watanabe, D., Pastan, I., Kobayashi, K., Nihira, T., Mochizuki, H., Yamada, S., Mori, K., and Yamaguchi, M. (2011). Compensation of depleted neuronal subsets by new neurons in a local area of the adult olfactory bulb. J. Neurosci. *31*, 10540–10557.

32. Takahashi, H., Ogawa, Y., Yoshihara, S., Asahina, R., Kinoshita, M., Kitano, T., Kitsuki, M., Tatsumi, K., Okuda, M., Tatsumi, K., et al. (2016). A subtype of olfactory bulb interneurons is required for odor detection and discrimination behaviors. J. Neurosci. *36*, 8210–8227.

33. David, L.S., Schachner, M., and Saghatelyan, A. (2013). The extracellular matrix glycoprotein tenascin-R affects adult but not developmental neurogenesis in the olfactory bulb. J. Neurosci. *33*, 10324–10339.

34. Mak, G.K., Enwere, E.K., Gregg, C., Pakarainen, T., Poutanen, M., Huhtaniemi, I., and Weiss, S. (2007). Male pheromone-stimulated neurogenesis in the adult female brain: possible role in mating behavior. Nat. Neurosci. *10*, 1003–1011.

35. Moreno, M.M., Linster, C., Escanilla, O., Sacquet, J., Didier, A., and Mandairon, N. (2009). Olfactory perceptual learning requires adult neurogenesis. Proc. Natl. Acad. Sci. USA *106*, 17980–17985.

36. Shingo, T., Gregg, C., Enwere, E., Fujikawa, H., Hassam, R., Geary, C., Cross, J.C., and Weiss, S. (2003). Pregnancy-stimulated neurogenesis in the adult female forebrain mediated by prolactin. Science *299*, 117–120.

37. Lisman, J., Schulman, H., and Cline, H. (2002). The molecular basis of CaMKII function in synaptic and behavioural memory. Nat. Rev. Neurosci. *3*, 175–190.

38. Benson, D.L., Isackson, P.J., Gall, C.M., and Jones, E.G. (1992). Contrasting patterns in the localization of glutamic acid decarboxylase and Ca2+/calmodulin protein kinase gene expression in the rat central nervous system. Neuroscience *46*, 825–849.

39. Jones, E.G., Huntley, G.W., and Benson, D.L. (1994). Alpha calcium/calmodulin-dependent protein kinase II selectively expressed in a subpopulation of excitatory neurons in monkey sensory-motor cortex: comparison with GAD-67 expression. J. Neurosci. *14*, 611–629.

40. De Koninck, P., and Schulman, H. (1998). Sensitivity of CaM kinase II to the frequency of Ca2+ oscillations. Science *279*, 227–230.

41. Giese, K.P., Fedorov, N.B., Filipkowski, R.K., and Silva, A.J. (1998). Autophosphorylation at Thr286 of the alpha calcium-calmodulin kinase II in LTP and learning. Science *279*, 870–873.

42. Lemieux, M., Labrecque, S., Tardif, C., Labrie-Dion, É., Lebel, É., and De Koninck, P. (2012). Translocation of CaMKII to dendritic microtubules supports the plasticity of local synapses. J. Cell Biol. *198*, 1055–1073.

43. Lledo, P.M., Hjelmstad, G.O., Mukherji, S., Soderling, T.R., Malenka, R.C., and Nicoll, R.A. (1995). Calcium/calmodulin-dependent kinase II and long-term potentiation enhance synaptic transmission by the same mechanism. Proc. Natl. Acad. Sci. USA *92*, 11175–11179.

44. Flores, C.E., Nikonenko, I., Mendez, P., Fritschy, J.-M., Tyagarajan, S.K., and Muller, D. (2015). Activity-dependent inhibitory synapse remodeling through gephyrin phosphorylation. Proc. Natl. Acad. Sci. USA *112*, E65–E72.

45. Marsden, K.C., Shemesh, A., Bayer, K.U., and Carroll, R.C. (2010). Selective translocation of Ca2+/calmodulin protein kinase IIalpha (CaMKIIalpha) to inhibitory synapses. Proc. Natl. Acad. Sci. USA *107*, 20559–20564.

46. Petrini, E.M., Ravasenga, T., Hausrat, T.J., Iurilli, G., Olcese, U., Racine, V., Sibarita, J.-B., Jacob, T.C., Moss, S.J., Benfenati, F., et al. (2014). Synaptic recruitment of gephyrin regulates surface GABAA receptor dynamics for the expression of inhibitory LTP. Nat. Commun. *5*, 3921.

47. Saliba, R.S., Kretschmannova, K., and Moss, S.J. (2012). Activity-dependent phosphorylation of GABAA receptors regulates receptor insertion and tonic current. EMBO J. *31*, 2937–2951.

48. Fritschy, J.M., and Mohler, H. (1995). GABAA-receptor heterogeneity in the adult rat brain: differential regional and cellular distribution of seven major subunits. J. Comp. Neurol. *359*, 154–194.

49. Farrant, M., and Nusser, Z. (2005). Variations on an inhibitory theme: phasic and tonic activation of GABA(A) receptors. Nat. Rev. Neurosci. *6*, 215–229.

50. Deshpande, A., Bergami, M., Ghanem, A., Conzelmann, K.-K., Lepier, A., Götz, M., and Berninger, B. (2013). Retrograde monosynaptic tracing reveals the temporal evolution of inputs onto new neurons in the adult dentate gyrus and olfactory bulb. Proc. Natl. Acad. Sci. USA *110*, E1152–E1161.

51. Nagayama, S., Homma, R., and Imamura, F. (2014). Neuronal organization of olfactory bulb circuits. Front. Neural Circuits *8*, 98.

52. Waclaw, R.R., Ehrman, L.A., Pierani, A., and Campbell, K. (2010). Developmental origin of the neuronal subtypes that comprise the amygdalar fear circuit in the mouse. J. Neurosci. *30*, 6944–6953.

53. Mantamadiotis, T., Lemberger, T., Bleckmann, S.C., Kern, H., Kretz, O., Martin Villalba, A., Tronche, F., Kellendonk, C., Gau, D., Kapfhammer, J., et al. (2002). Disruption of CREB function in brain leads to neurodegeneration. Nat. Genet. *31*, 47–54.

54. Drobizhev, M., Tillo, S., Makarov, N.S., Hughes, T.E., and Rebane, A. (2009). Absolute two-photon absorption spectra and two-photon brightness of orange and red fluorescent proteins. J. Phys. Chem. B *113*, 855–859.

55. Veilleux, I., Spencer, J.A., Biss, D.P., Cote, D., and Lin, C.P. (2008). In vivo cell tracking with video rate multimodality laser scanning microscopy. IEEE J. Sel. Top. Quantum Electron *14*, 10–18.

56. Scotto-Lomassese, S., Nissant, A., Mota, T., Néant-Féry, M., Oostra, B.A., Greer, C.A., Lledo, P.-M., Trembleau, A., and Caillé, I. (2011). Fragile X mental retardation protein regulates new neuron differentiation in the adult olfactory bulb. J. Neurosci. *31*, 2205–2215.

KEY RESOURCES TABLE

REAGENT or RESOURCE	SOURCE	IDENTIFIER
Antibodies		
Mouse monoclonal anti-CaMKIIα	ThermoFisher Scientific	Cat# MA1-048; RRID: AB_325403
Rabbit polyclonal anti-c-Fos	Santa Cruz Biotechnology	Cat# sc-52; RRID: AB_2106783
Rabbit polyclonal anti-GFP	ThermoFisher Scientific	Cat# A-11122; RRID: AB_221569
Chicken polyclonal anti-GFP	Avés	GFP-1020; RRID: AB_10000240
Rabbit monoclonal anti-NeuN	Cell Signaling	Cat# 12943; RRID: AB_2630395
Rabbit polyclonal anti-mCherry	BioVision	Cat # 5993-100; RRID: AB_1975001
Bacterial and Virus Strains		
AAV 2/1-CBA-GFP	Molecular Tool Platform CERVO Brain Research center	Lot # AAV 19
AAV 2/1 -CaMKIIα-GFP	Molecular Tool Platform CERVO Brain Research center	Lot # AAV 36
AAV 2/5-CaMKIIa-HA-hM4D(Gi)-IRES-mCitrine	University of North Carolina Vector Core Facility	Lot # AV4617d
AAV 2/5-CAG-GCαMP6s-WPRE-SV40	University of Pennsylvania Vector Core Facility #AV-5-PV2833	Cat #AV-5-PV2833
AAV 2/5 -EF1 α-DIO-EYFP	University of North Carolina Vector Core Facility	Lot # AV4310J
AAV 2/5 -CAG-FLEX-tdTomato	University of North Carolina Vector Core Facility	Lot # AV4599
AAV 2/5-hSyn-EGFP	Addgene	Cat # 50465-AAV5
AAV 2/5-hSyn-HA-hM4D(Gi)-mCherry	Addgene	Cat # 50475-AAV5
AAV 2/5- CaMKIIα-mCherry-Cre	University of North Carolina Vector Core Facility	Lot # AV6448b
LV -EF1α-Cre-mCherry-Puro	SignaGen Laboratories	Cat # SL100281
LV-GFP	Ecole des Neuroscience platform (ENP), Paris	N/A
Chemicals, Peptides, and Recombinant Proteins		
Butyraldehyde	Sigma-Aldrich	538191; CAS: 123-72-8
Ethyl tiglate	Sigma-Aldrich	W246018; CAS: 5837-78-5
Valeric Acid	Sigma-Aldrich	75054; CAS: 109-52-4
Isoamyl acetate	Sigma-Aldrich	W205508; CAS: 123-92-2
(+)-carvone	Sigma-Aldrich	22070; CAS: 2244-16-8
(-)-carvone	Sigma-Aldrich	22060; CAS: 6485-40-1
Decanal	Sigma-Aldrich	59581; CAS: 112-31-2
Octyl aldehyde (octanal)	Sigma-Aldrich	5608; CAS: 124-13-0
(R)-(+)-limonene	Sigma-Aldrich	62118; CAS: 5989-27-5
(S)-(-)-limonene	Sigma-Aldrich	62128; CAS: 5989-54-8
Sunflower seed oil	Sigma-Aldrich	47123; CAS: 8001-21-6
Mineral oil	Sigma-Aldrich	M5904; CAS: 8042-47-5
Paraformaldehyde	Sigma-Aldrich	P6148; CAS: 30525-89-4
Kynurenic acid	Sigma-Aldrich	K3375; CAS: 492-27-3
Biccuculine Methiodine	Abcam	ab120108
Tetrodotoxin	Affix Scientific	AF3015; CAS: 4368-28-9
Clozapine-N-Oxide	Tocris Bioscience	4936; CAS: 34233-69-7
Tamoxifen	Sigma-Aldrich	T5648; CAS: 10540-29-1

REAGENT or RESOURCE	SOURCE	IDENTIFIER
Anhydrous ethyl alcohol	Commercial Alcohols	1019C
Experimental Models: Organisms/Strains		
Mouse: NestinCreERT2	[13]	N/A
Mouse: CAG-CAT-EGFP	[52]	N/A
Mouse: NestinCreERT2::CC-GFP	This paper	N/A
Mouse: CamkCre4	[53]	N/A
Mouse: B6;129S6-$Gt(ROSA)26Sor^{tm14(CAG\ tdTomato)Hze}$J (CAG-tdTomato)	The Jackson Laboratory	Cat# JAX:007908; RRID:IMSR_JAX: 007908
Mouse: CD1	Charles River	Strain code: 022
Mouse: C57BL/6NCRL	Charles River	Strain code: 027
Software and Algorithms		
MATLAB 2016a	The MathWorks	https://www.mathworks.com/
MATLAB scripts for Ca^{2+} imaging analysis	This paper	N/A
ImageJ	NIH	https://imagej.net/Welcome
Huygens	Scientific Volume Imaging	https://svi.nl/HuygensSoftware
NeuronStudio	Computational Neurobiology and Imaging center	http://research.mssm.edu/cnic/tools-ns.html
Mini Analysis	Synaptosoft	http://www.synaptosoft.com/
Other		
Polyethylene tubing (PE50, I.D. 0.58 mm, O.D. 0.965 mm)	Becton Dickinson	427517
Vicryl suture (3-0)	Johnson & Johnson	J442H
4-channel olfactometer	Knosys	http://www.knosysknosys.com/

CONTACT FOR REAGENT AND RESOURCE SHARING

Further information and requests for resources and reagents should be directed to and will be fulfilled by the Lead Contact, Armen Saghatelyan (armen.saghatelyan@fmed.ulaval.ca).

EXPERIMENTAL MODEL AND SUBJECT DETAILS

Adult (>2-month-old) male C57BL/6 mice (Charles River) were used for most experiments. NestinCreERT2::CAG-CAT-EGFP (NestinCreERT2::CC-GFP) mice were used to study the expression of CaMKIIα in adult-born neurons. These mice were obtained by crossing NestinCreERT2 mice [13] with CAG-CAT-EGFP mice [52]. They received daily injections of tamoxifen (180 mg/kg, Sigma Aldrich) for 5 days to induce the expression of GFP by stem cells and their progeny. Tamoxifen was diluted in sunflower seed oil (Sigma Aldrich) and 10% anhydrous ethanol. Postnatal day 5 (P5) CD1 mice (Charles River) were used to compare the morphological characteristics of early-born GCs. The experiments were performed in accordance with Canadian Guide for the Care and Use of Laboratory Animals guidelines and were approved by the Animal Protection Committee of Université Laval. The mice were kept in groups of 4-5 on a 12-h light/dark cycle in a temperature-controlled facility (22°C), with food and water ad libitum, except for the mice in go/no-go odor discrimination and long-term associative memory groups, which were partially water- and food-deprived, respectively. Animals that underwent behavioral procedures were individually housed and kept on a reverse light-dark cycle for 7-10 days before beginning the experiments. Animals were randomly assigned to the various experimental groups.

To genetically label CaMKIIα⁺ cells, the CamkCre4 [53] and CAG-tdTomato (http://jaxmice.jax.org/strain/007908.html) mouse transgenes were backcrossed to C57BL/6 and 129/SvPas genetic backgrounds, respectively. Hemizygous CamkCre4$^{+/0}$ and CAG-tdTomato$^{+/0}$ mice were then crossed to obtain double transgenic F1 offspring (CaMKIIα-tdTomato). All mice were individually housed in ventilated cages under specific pathogen-free conditions at 22°C and a 12-h light/dark cycle, with food and water ad libitum. The experiments were approved by the Charles Darwin University Animal Ethics Committee (approvals Ce5/ 2012/074 and C2EA-05).

METHOD DETAILS

Stereotaxic injections
We used adeno-associated viral vectors (AAVs) to label neuronal precursors to assess the electrophysiological properties of GCs. The AAVs were produced at the Molecular Tools Platform of the CERVO Research Center. The mice were stereotaxically injected in the RMS

with either a control vector (GFP under the chicken β-actin CBA promoter; CBA-GFP) to label neuronal precursors regardless of their molecular characteristics or a CaMKIIα-specific vector (GFP under the CaMKIIα promoter; CaMKIIα-GFP) to infect precursors that differentiate into CaMKIIα+ GCs. The stereotaxic injections were performed under ketamine/xylazine anesthesia (10 mg/mL and 1 mg/mL respectively; 0.1 mL per 10 g of body weight) at the following coordinates (with respect to the bregma): anterior-posterior (AP) 2.55, medio-lateral (ML) 0.82, and dorso-ventral (DV) 3.15. The mice were allowed to recover and were returned to their home cages.

For the morphological analyses of adult-born GCs, the SVZs of C57BL/6 mice were injected with a GFP-expressing lentivirus at the following coordinates AP: 1, ML: 1, DV: 2.1. They were sacrificed 14, 21, and 28 days after the injections (n = 4 mice per time-point).

For the morphological analyses of early-born GCs, the OBs of CD1 P5 mice were injected with a mixture of EF1α-Cre-mCherry lentivirus (SignaGen Laboratories, 3.88×10^9 TU/mL) and EF1α-DIO-EYFP AAV (University of North Carolina Vector Core Facility, 6.5×10^{12} TU/mL) at a ratio of 0.2/0.8. The low amount of Cre virus made it possible to sparsely label GCs and thus to accurately assess their dendritic morphology and spine density.

Cranial window surgery and in vivo two-photon calcium imaging

Adult mice were injected with a mixture of three different AAV vectors (at a ratio of 1:1:1) to allow the simultaneous comparison of Ca^{2+} activity in CaMKIIα+ and general population of GCs (composed of CaMKIIα+ and CaMKIIα-). We used AAV-CAG-GCaMP6s-WPRE-SV40 (University of Pennsylvania Vector Core Facility, 2.23×10^{13} iu/mL), AAV-CAG-FLEX-tdTomato (University of North Carolina Vector Core Facility, 8×10^{12} iu/mL), and AAV-CaMKIIα-Cre-mCherry (University of North Carolina Vector Core Facility, 4.8×10^{12} iu/mL). Co-injection of the CaMKIIα-Cre-mCherry and CAG-Flex-tdTomato AAV vectors boosted the red fluorescence signal in co-infected CaMKIIα+ GCs. Furthermore, tdTomato is more suitable for multi-photon imaging than mCherry at the excitation wavelength we used (1040 nm) [54]. The viruses were injected bilaterally in the OB at the following coordinates (with respect to the bregma): AP 5.3, ML 0.5, DV 0.9; and AP 4.6, ML 0.75, DV 1.0. Two to four weeks post-viral infection, cranial window surgery was performed as previously described [24]. The mice were anesthetized with 2%–3% isoflurane, and their body temperature was maintained at 37.5°C using an infrared heating blanket (Kent Scientific). After removing the skin, a circular craniotomy centered over the OB was drilled and the bone was removed, leaving the dura mater intact. A 3-mm-diameter glass coverslip was put on the top surface of the OB, and Kwik-Seal (World Precision Instruments) and Metabond cement (Parkell Inc.) were used to fix the coverslip in place. During the procedure, a custom-made head plate was also attached to the skull in order to prevent the animal's head from moving during imaging. At the end of the surgery, the isoflurane concentration was gradually decreased. The mice were kept under ketamine/xylazine anesthesia for the entire imaging session.

A custom-built video-rate two-photon microscope was used to image Ca^{2+} activity in the GC subtypes [55]. The mouse was positioned under the microscope using the head plate on a custom-made stereotaxic frame controlled by a micromanipulator (MPC 200; Sutter). A 20x water-immersion objective (XLUMPlanFl 20x/numerical aperture (NA) 0.95; Olympus) was used to locate the region of interest (ROI). A Ti:Sapphire tunable laser (Mai Tai; Spectra Physics) with a wavelength of 920-940 nm was used to excite GCaMP6s, and a 1040 nm HighQ-2 laser (Spectra Physics) was used to excite tdTomato and reveal the GC subtypes. Ca^{2+} activity in the GCs was imaged using a 60x water immersion objective (LUMPlanFl/IR 60x/NA 0.9). GCs were identified by their smaller size and their location in the GCL. Several ROIs were selected, and baseline activity was recorded in these regions during 2 min acquisitions at a frame rate of 30-32 Hz. Odor-evoked responses were then recorded in the same ROIs. Odors were delivered for 5 s using a custom-made olfactometer. Odor delivery was preceded by 10 s imaging of baseline fluorescent activity of GCaMP6s-infected cells. Six different odorants (butyraldehyde, methylbenzoate, ethyltiglate, valeric acid, isoamylacetate, (+)-carvone; Sigma Aldrich) were diluted in mineral oil to a final concentration of 1% v/v. These odorants were chosen because they activate the medio-lateral part of the dorsal surface of the OB [6, 24, 25]. Each odor was presented three times, with a 1-2 min inter-trial interval. Since it has been shown that mice respond with a higher sniffing rate to the first application of each odor [23], only the second and third trials of odor application were retained for analysis. The responses of the second and third trials were averaged. No correction for neuropil fluorescence was applied.

Immunohistochemistry

The mice were deeply anesthetized using an intraperitoneal injection of sodium pentobarbital (12 mg/mL; 0.1 mL per 10 g of body weight) and were intracardiacally perfused with 0.9% NaCl followed by 4% paraformaldehyde (PFA). The brains were collected and were post-fixed overnight in 4% PFA. Coronal or horizontal 50 or 100-μm-thick OB sections were cut using a vibratome (Leica) and were incubated with the following primary antibodies: rabbit anti-cFos (SC-52, 1:40,000, 48 h; Santa Cruz), mouse anti-CaMKIIα (MA1-048, 1:500, 48 h; ThermoFisher Scientific), rabbit anti-NeuN (D3S31, 1:500; 24 hr, Cell Signaling), rabbit anti-GFP (A-11122, 1:1000, 24 h; ThermoFisher Scientific), chicken anti-GFP (GFP-1020, 1:1000, 24 h; Aves) or rabbit anti-mCherry (5993-100, 1:1000; 24 h; Biovision). The antibodies were diluted in either 0.5% Triton X-100 and 4% milk or 0.3% Triton X-100 and 10% FBS prepared in PBS. The corresponding secondary antibodies were used. Fluorescence images were acquired using a confocal microscope (FV 1000; Olympus) with 60x (UPlanSApoN 60x/NA 1.42; Olympus) and 40x (UPlanSApoN 40x/NA 0.90; Olympus) oil and air immersion objectives, respectively.

Morphological analysis

The morphologies of 14, 21, and 28-d post-injection (dpi) adult-born and 18 dpi early-born neurons were determined as previously described [28, 33, 56]. To distinguish the two GC populations, CaMKIIα immunostaining was performed. Images were acquired with a LSM 700 AxioObserver confocal microscope using 40x objective. For spine density quantification, images were zoomed 4 times.

Electrophysiological recordings

Two to three weeks after the stereotaxic injection of either a control CBA-GFP AAV or a CaMKIIα-GFP AAV, the mice were deeply anesthetized and were perfused transcardiacally with ice-cold sucrose-based artificial cerebro-spinal fluid (ACSF) containing the following (in mM): 250 sucrose, 3 KCl, 0.5 CaCl$_2$, 3 MgCl$_2$, 25 NaHCO$_3$, 1.25 NaH$_2$PO$_4$, and 10 glucose. The brains were quickly collected and were immersed in ACSF. Horizontal 250-μm-thick OB slices were obtained using a vibrating blade microtome (HM 650V; Thermo Scientific). The slices were transferred into oxygenated ACSF maintained at 32°C containing the following (in mM): 124 NaCl, 3 KCl, 2 CaCl$_2$, 1.3 MgCl$_2$, 25 NaHCO$_3$, 1.25 NaH$_2$PO$_4$, and 10 glucose. Inhibitory postsynaptic currents (IPSCs) and excitatory postsynaptic currents (EPSCs) were recorded using a Multiclamp 700A amplifier (Molecular Devices). We opted for recordings from virally labeled CBA-GFP GCs that, unlike recordings from the CaMKIIα-GFP-negative population (not labeled virally), allowed us to select GCs that had preserved dendritic morphology based on the expression of GFP. Patch electrodes with resistances ranging from 7 to 9 MΩ were filled with a CsCl-based intracellular solution to record inhibitory currents from GFP-labeled GCs. The intracellular solution contained the following (in mM): 135 CsCl, 10 HEPES, 0.2 EGTA, 2 ATP, 0.3 GTP, and 10 glucose (pH ≈ 7.2). The access resistance was continuously monitored, and recordings with a >15% change were discarded. The GCs were kept at –60 mV. Spontaneous IPSCs (sIPSCs) were isolated by bath applying 5 mM kynurenic acid (Kyn) to block glutamatergic activity. Miniature IPSCs (mIPSCs) were isolated by applying 1 μM tetrodotoxin (TTX) to block voltage-sensitive sodium channels in the presence of 5 mM Kyn. To record EPSCs, the patch electrodes were filled with a K-methylsulfate-based intracellular solution containing the following (in mM): 130 K-methylsulfate, 10 HEPES, 6 KCl, 2 ATP, 0.4 GTP, 10 Na-phosphocreatine, and 2 ascorbate (pH ≈ 7.2). Spontaneous EPSCs (sEPSCs) were isolated by bath applying 50 μM biccuculine methiodide (BMI) to block GABA$_A$ receptors. Miniature EPSCs (mEPSCs) were isolated by applying 1 μM TTX to block voltage-sensitive sodium channels in the presence of 50 μM BMI. Spontaneous synaptic events were analyzed during 2 min of continuous recording using the Mini analysis program (Synaptosoft). The analysis was blinded to the experimental group.

Novel odor stimulation

The mice were separated into two groups. Each mouse was individually housed in a clean cage and spent 1 hr with no odor. The two groups were then presented for 1 hr with two tea balls suspended in the cage. For the control group, the tea balls were filled with a filter paper alone, whereas for the experimental group, the tea balls were filled with a filter paper soaked with 100 μl of pure (+)-limonene and (-)-limonene. The tea balls were then removed, and the animals were perfused with 4% PFA 1 hr later. The density of cFos$^+$ cells and the percentage of CaMKIIα$^+$/cFos$^+$ and CaMKIIα$^+$/DAPI$^+$ cells were determined blindly to the experimental condition.

Sensory deprivation

Occlusion plugs were fabricated using polyethylene tubing (PE50, I.D. 0.58 mm, O.D. 0.965 mm; Becton Dickinson), with the center blocked using a tight-fitting Vicryl suture knot (3-0; Johnson & Johnson). The ~5-mm-long petroleum jelly-coated plugs were inserted in the left nostril of four mice under isoflurane anesthesia. The mice were sacrificed by intracardiac perfusion 1 day later.

Behavioral procedures
Odor discrimination

For the odor discrimination task based on habituation/dishabituation, the odors were presented in glass Pasteur pipettes containing filter paper soaked with 6 μL of 2% odorant in mineral oil. The odor presentations consisted of 5 min sessions separated by 20 min intervals. The mice were first habituated to the glass pipette by presenting it to them twice. They were then subjected to four habituation sessions with a first odor ((+)-carvone; Sigma Aldrich). One group of animals (control group) was subjected to a fifth session with the same habituation odor. A second group of animals (habituation/dishabituation group) was subjected to a second odor (dishabituation odor, (-)-carvone; Sigma Aldrich). The time spent exploring the pipette during each session was recorded. The mice from the two groups were sacrificed 1 hr after completing the task by intracardiac perfusion with 4% PFA. Fifty-μm-thick OB coronal slices were cut and immunolabeled for cFos and CaMKIIα.

Perceptual learning

The mice were exposed in their home cages to two tea balls for 1 hr per day for 10 consecutive days. One tea ball contained 100 μL of pure (+)-limonene and the other contained 100 μL of pure (-)-limonene. On day 11, the mice were separated into two groups. One group was placed in a clean cage, and the mice were sacrificed after 1 hr (Learning group). The second group (Learning + Odor re-exposure group) was placed in a clean cage and was exposed to the odorants for 1 hr. The mice were then transferred to a clean cage and were sacrificed after 1 hr.

Go/no-go olfactory discrimination learning

The mice were partially water-deprived until they reached 80%–85% of their initial body weight prior to starting the go/no-go training. They underwent training sessions to habituate them to the cage of the olfactometer and to learn how to get a water reward. The mice were trained using 20 trials, with no exposure to an odor, to insert their snouts into the odor sampling port and to lick the water port to receive a 3 μL water reward. The ports were located side-by-side. The reward-associated odor (0.1% octanal; S+) was then introduced. Inserting the snout into the odor sampling port broke a light beam and opened an odor valve. The duration of the opening was increased gradually from 0.1 to 1 s over several sessions, and the mice with a minimum sampling time of 50 ms were given a water

reward. The mice usually completed this training after one or two 30 min sessions. Once they had successfully completed this training step, the mice were subjected a go/no-go odor discrimination test. Prior to being introduced to the odor not associated with a reward (0.1% decanal; S-), the mice underwent an introductory S- session consisting of exposure to S+ for 30 trials. If the success rate was at least 80%, the discrimination task was begun. The mice were then exposed randomly to S+ or S-, and the percentage of correct responses was calculated for each block of 20 trials. If a mouse licked the water port after being exposed to S+ (hit) and did not lick the water port after being exposed to S- (correct rejection), this was recorded as a correct response. A false response was recorded if the mouse licked the water port after being exposed to S- or if it did not lick the water port after being exposed to S+. A mouse was considered successful if it reached the criterion score of 80%. The control group underwent the same go/no-go procedure but received the water reward independently of the odor used (S+ or S-). The mice from the two groups were sacrificed 1 hr after completing the task by intracardiac perfusion with 4% PFA. Fifty-μm-thick OB coronal slices were cut and were immunolabeled for cFos and CaMKIIα. The density of cFos$^+$ cells and the percentage of CaMKIIα^+/cFos$^+$ and CaMKIIα^+/DAPI$^+$ cells were blindly determined.

Long-term associative memory

The mice used for this task were deprived of food for four to five days before beginning the test as well as during the learning period to reduce their initial body weight by 15%–20%. The test was performed as described previously [20, 21]. Briefly, during the first training period, the mice underwent four 10 min sessions a day. For two of the sessions, the first odor (15% (+)-carvone in mineral oil) was presented in association with a sugar reward. For the other two sessions, the second odor (15% (-)-carvone in mineral oil) was presented with no reward. For the control group (pseudo-conditioned mice), the sugar reward was randomly presented with either (+)-carvone or (-)-carvone. Associative memory was assessed 24 hr after the last training session. The mice were then re-exposed to both odors with no sugar reward and were allowed to explore them for 5 min. The time spent clawing the bedding above each odor was recorded. The density of cFos$^+$ cells and the percentage of CaMKIIα^+/cFos$^+$ and CaMKIIα^+/DAPI$^+$ cells were blindly determined.

Pharmacogenetic inactivation of CaMKIIα^+ GCs

We inactivated the GCs using the Designer Receptors Exclusively Activated by Designer Drugs (DREADD) pharmacogenetic approach to investigate the roles of different subtypes of GCs in odor behavior [29]. The mice were separated into different groups and received a stereotaxic injection of either a control (CaMKIIα-GFP or Syn-GFP) or a CaMKIIα-specific DREADD (CaMKIIα-HA-hM4D(Gi)-IRES-mCitrine; University of North Carolina Vector Core Facility; 2x10^{12} iu/mL) or a Synapsin-specific DREADD (hSyn-HA-hM4D(Gi)-mCherry) AAV (Addgene; 3x10^{12} iu/mL). No differences in the behavioral performances of two control groups injected either with CaMKIIα-GFP or Syn-GFP were observed and the data were thus pooled. The injections were performed bilaterally in the OB at two different sites at the following coordinates (with respect to the bregma): AP 5.3, ML 0.5, DV 0.9; and AP 4.6, ML 0.75, DV 1.0. Three to four weeks post-injection, the mice were tested using the odor discrimination habituation/dishabituation, go/no-go operant conditioning, or perceptual learning task. To investigate the effect of CaMKIIα^+ GC activity inhibition on habituation/dishabituation odor discrimination performances, mice from the two groups received an intraperitoneal injection of clozapine-N-oxide (CNO, 2 mg/kg of body weight in 0.9% NaCl; Tocris Bioscience) 30 min before the dishabituation odor was presented. For the go/no-go odor discrimination learning task, the mice from the two groups received the CNO injection 30 min before the test. No treatment was given during the training period. For the perceptual learning task, the mice received daily injections of CNO during the 10-day odor enrichment period 30 min before being exposed to the odors. No treatment was given on day 11.

For the perceptual learning task, the mice were tested using an odor discrimination task before and after a 10-day enrichment procedure, as previously described [28]. After an initial 50 s presentation of mineral oil, the mice underwent four consecutive 50 s presentations of the habituation odor ((+)-limonene) at 5 min intervals. The dishabituation odor ((-)-limonene) was presented for 50 s during the fifth session, and the exploration time was measured. After 10 days of olfactory enrichment and the CNO treatment, the mice were retested using the same task (i.e., post-enrichment test). All pharmacogenetic experiments were performed with the investigator blinded to the experimental condition.

QUANTIFICATION AND STATISTICAL ANALYSIS

Cell morphology was analyzed using the simple neurite tracer and cell counter plugins in ImageJ or with NeuronStudio software. To determine the percentage of CaMKIIα^+ or tdTomato$^+$ GCs among the Dapi+ or NeuN+ cells, as well as the density of cFos$^+$ GCs, the counting was performed using images acquired with 63x or 40x objectives with 1-μm-thick optical sections. At least three coronal slices derived from the anterior, medial, and posterior portion of the OB (in the rostro-caudal axis) from each individual animal were used. Images were acquired from the medial, lateral, and ventral portions of the GCL to avoid regional bias in cFos expression. cFos cells in the field were identified, and co-labeling for CaMKIIα or tdTomato was evaluated in consecutive optical sections. The investigator was blinded to the experimental conditions in most immunohistochemical quantifications (novel odor presentation, long-term associative memory, go/no-go olfactory discrimination learning).

Ca^{2+} responses were analyzed using a custom-written script in MATLAB (The MathWorks). GCaMP6s and RFP (tdTomato and mCherry) video-rate image stacks (30 ms/frame) were recorded for the XY positions and were corrected for brain motion using the StackReg ImageJ plugin. The aligned stacks were time-averaged in 1 s bins. To remove out-of-focus frames and quantify

GCaMP6s GC activity, we used a custom-written script in MATLAB that allowed us to select the z planes based on the homology between the frames of the RFP channel. The script computed the average normalized cross-correlation peak for the complete image stack. The frames with the highest peak correlation values were considered in focus, whereas the frames with peak correlation values lower than a user-defined threshold (set at 1%) were removed. ROIs in each cell were manually drawn to extract the GCaMP6s fluorescence signal over the entire cell body. The background signal was measured in at least three different regions of the movie and was subtracted from the Ca^{2+} traces in the cells. For experiments assessing Ca^{2+} activity under baseline conditions, all peaks with amplitude greater than 2.5 times that of the mean standard deviation (SD) of each trace were retained. Several thresholds (1xSD, 1.5xSD, 2xSD, 2.5xSD) were empirically tested by visually inspecting Ca^{2+} activity and by determining whether motion-induced negative deflections in the ΔF/F traces could be detected. For the odor stimulation experiments, we calculated the ΔF/F value, and the response threshold was defined as 2.5xSD of the fluorescence intensity of the pre-odor value. If the peak fluorescence intensity during the odor stimulation was higher than the response threshold, the cell was classified as an 'ON' cell. If the peak fluorescence intensity of the post-odor period (occurring up to 5 s after the end of odor stimuli) was higher than the response threshold, the cell was classified as an 'OFF' cell. These periods were chosen based on a previous report showing that the temporal dynamic of mitral cell responses to odors is diverse, spanning the 5 s period of odor presentation and a few seconds after the odor offset [23], and the fact that responses recorded in GCs were one synapse away from those recorded in mitral cells. Non-responsive cells were also logged in the analysis to calculate the percentage of ON and OFF responses and odor tuning. Odor tuning responses were analyzed using a custom-written MATLAB script. This algorithm labels all cells in the imaging region and localizes them through different acquisitions of the six odors presented. A template containing all the cells is then created by summing the binary images of every acquisition. The Ca^{2+} responses of GCs to each individual odor that had been analyzed using the custom-written MATLAB script were compiled in a file by matching the coordinates of cells in the summed and individual binary images, and the odor tuning responses were calculated.

Data are expressed as means ± SEM. When possible, the investigator was blinded to the experimental conditions as specified in Methods details. Statistical significance was determined using a paired or unpaired two-sided Student's t test, or Kolmogorov-Smirnov test depending on the experiment, as indicated in the text and corresponding figure legends. The exact value of n and its representation (cells, animals) is indicated in the text and corresponding figure legends. No statistical methods were used to predetermine the sample size. Equality of variance for the unpaired t test was verified using the F-test. The levels of significance were as follows: $^*p < 0.05$, $^{**}p < 0.01$, $^{***}p < 0.001$.

DATA AND SOFTWARE AVAILABILITY

The data supporting the findings and the MATLAB scripts used for analysis are available upon request.

Supplemental Information

CaMKIIα Expression Defines Two Functionally

Distinct Populations of Granule Cells Involved

in Different Types of Odor Behavior

Sarah Malvaut, Simona Gribaudo, Delphine Hardy, Linda Suzanne David, Laura Daroles, Simon Labrecque, Marie-Anne Lebel-Cormier, Zayna Chaker, Daniel Coté, Paul De Koninck, Martin Holzenberger, Alain Trembleau, Isabelle Caille, and Armen Saghatelyan
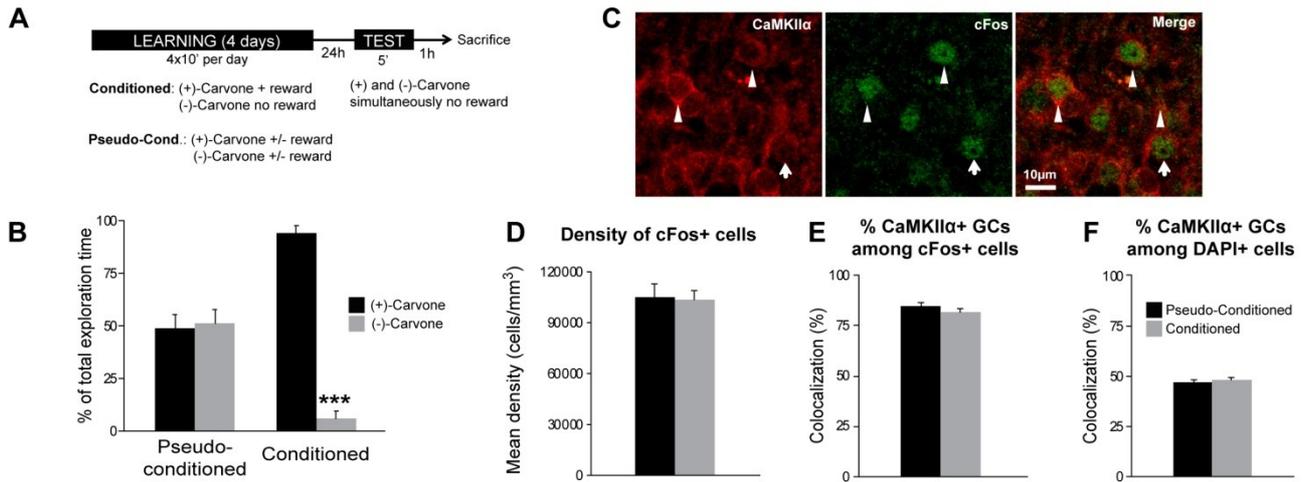
Figure S1: GCs subtypes activation during long-term associative memory, Related to Figure 7

A. Experimental design of the long-term associative memory task. **B.** Long-term associative memory behavioral results after the 24-h task. Mice from the pseudo-conditioned group (n=5) spent the same percentage of time exploring both odorants. Conditioned mice (n=10) expressed a clear preference for the odorant previously associated with the odor reward. ***$p<0.001$ paired Student's *t*-test. **C.** CaMKIIα (red) and cFos (green) immunolabeling. The arrows indicate a CaMKIIα⁻ GC. The arrowheads indicate a CaMKIIα⁺ GC. **D.** No difference in the density of cFos⁺ GCs was observed between the two groups. **E.** No change in the percentage of cFos⁺/CaMKIIα⁺ GCs was observed after the long-term associative learning task (pseudo-conditioned: n=291 cells, n=3 mice; conditioned: n=397 cells, n=4 mice). **F.** Percentage of DAPI⁺/CaMKIIα⁺ GCs (pseudo-conditioned: n=841 cells, n=3 mice; conditioned: n=1587 cells, n=5 mice).